Thin-Walled Structures 183 (2023) 110390

Contents lists available at ScienceDirect

Thin-Walled Structures

journal homepage: www.elsevier.com/locate/tws

Evaluation of the composite action of cold-formed steel built-up battened columns composed of two sigma-shaped sections

Rohola Rahnavard [a,*], Mahtabsadat Razavi [b], Nader Fanaie [b], Hélder D. Craveiro [a,*]

[a] University of Coimbra, ISISE, Department of Civil Engineering, Coimbra, Portugal
[b] Department of Civil Engineering, K. N. Toosi University of Technology, Tehran, Iran

ARTICLE INFO

Keywords:
Cold-formed steel
Optima number of fasteners
Optima distance
Composite action
Battened columns
Batten panel

ABSTRACT

Cold-formed steel (CFS) built-up battened columns are employed to obtain a sufficient load-bearing capacity when individual profiles cannot withstand the specified stresses. This sufficient load-bearing capacity can be obtained when the individual profiles present a composite action. This paper presents the optimal layout for CFS built-up battened columns to achieve a high level of composite action between two Σ-shaped CFS profiles. A calibrated finite element modeling technique was used to evaluate the effect of the number of fasteners per batten panel and the distance between the batten panels on the axial capacity of CFS built-up battened columns. The optimal number of fastener rows and the distance between the batten panels were determined using 100 models, in which a high level of composite action was achieved between CFS profiles. Then the maximum axial load-bearing capacity of additional 600 finite element models using the optimal layout was compared with the analytical predictions in the European standard EN1993-1-1. The results recommended four rows of fasteners per batten panel. The results suggested an optimal distance of $30i_{min}$ between batten panels. The results showed a close agreement between finite element and analytical predictions from EN1993-1-1, following the procedure specified in clause 6.3.1, adopting the modified slenderness ratio from the American Specification AISI S100-16. Reliability analysis was also performed to evaluate the analytical methods by targeting a reliability index of 2.5. The results showed that the analytical prediction following the EN1993-1-1, clause 6.3.1, incorporated with the recommended slenderness ratio from the AISI S100-16, is a reliable analytical procedure for CFS battened columns.

1. Introduction

As an effective substitute for hot-rolled steel, cold-formed steel (CFS) has been widely used in various structural applications in recent years. Lighter, stronger, more environmentally friendly, and less expensive to maintain are just some benefits CFS-built structures provide over their hot-rolled alternatives. Moreover, the CFS built-up sections cover various applications such as columns, beams, and even diagonally strap-braced stud walls [1–4]. The cold-formed steel profiles have high strength-to-weight ratios; however, their load-bearing capacity is relatively low. This low load-bearing capacity is due to their thin walls and sensitivity to local buckling phenomena. CFS profiles' potential low load-bearing capacity can be addressed using the possibility of combining multiple individual shapes known as CFS built-up sections. CFS built-up sections are usually created by fastening individual sections together. Another way to create CFS built-up sections is to connect individual profiles using batten panels. CFS built-up While individual profiles may be used to develop an extensive range of built-up members with various cross-section shapes and capabilities, fundamental knowledge of how these sections behave is still restricted. Because CFS built-up sections are composed of individual profiles and batten plates connected by fasteners, the buckling modes and interactions are very different from those seen in individual profiles. Furthermore, the distance between the batten panels and the number of fasteners per batten panel can impact the prevalent buckling modes and the actual efficiency of the composite action between the existing profiles. Because accounting for partial or full composite action is essential when working with built-up battened columns, developing tailored design methods must be used in practice.

Despite the various advantages of CFS built-up battened sections, the available design codes [5,6] rarely provide specialized design instructions. Even though EN 1993-1-3 [5] offers a global buckling curve for calculating the buckling resistance of a limited number of individual and built-up sections, it does not include particular design requirements for built-up battened sections. While critical parameters such as the maximum distance between the batten panels and the optimal number of fasteners per batten panel can significantly influence the behavior of CFS built-up battened columns, there are no specific criteria to

* Corresponding authors.
E-mail addresses: rahnavard@uc.pt, rahnavard1990@gmail.com (R. Rahnavard), heldercraveiro.eng@uc.pt (H.D. Craveiro).

https://doi.org/10.1016/j.tws.2022.110390
Received 19 July 2022; Received in revised form 12 October 2022; Accepted 20 November 2022
Available online xxxx

Notation

A	Area of a cross section
A_{ch}	Cross-sectional area of one chord
A_{eff}	Effective area of a cross section
E	Modulus of elasticity
I	Second moment of area of a cross section
I_{bp}	Second moment of area of one batten panel
C_p	Correction factor in reliability analysis
I_{ch}	Second moment of area of one chord
I_{eff}	Effective second moment of area of a cross-section
K	Spring stiffness per unit length of a stiffener
L	Length of a member
L_e	Effective length of a member
$N_{b,Rd}$	Design buckling resistance of a compression member
$N_{c,Rd}$	Design resistance of steel cross-section under compression
N_{cr}	Elastic buckling force
$N_{cr,B}$	Elastic flexural buckling force of a battened compression built-up member
$N_{cr,eff}$	Elastic flexural buckling force of a battened compression effective built-up member
$N_{cr,F}$	Elastic flexural buckling force
$N_{cr,T}$	Elastic torsional buckling force
$N_{cr,TF}$	Elastic torsional–flexural buckling force
S_v	Shear stiffness of a built-up battened member
d_{bp}	Distance between batten panels
M_m, F_m, V_M, and V_F	Statistical parameters in the reliability analysis
V_Q	Coefficient of the variation of the mean load effect in the reliability analysis
n	Number of models in reliability analysis
m	Degree of freedom in the reliability analysis
d_f	Distance between fasteners in the direction of load transfer
f_y	Yield strength
e_1	The end distance from the center of the fastener to the adjacent end of the batten panel, in the direction of load transfer
e_2	The edge distance from the center of the fastener to the adjacent end of the batten panel, perpendicular to the direction of load transfer
b	Width of a cross-section, plate width
h	Height of a cross-section
h_0	Distance between the centroids of chords
n_b	Number of batten panels
r	Radius of gyration of a cross-section
r_i	Minimum radius of gyration of the full unreduced cross-sectional area of an individual shape in a built-up member
t	Plate thickness
Φ_c	Safety factors for the available axial strength based on the Limit States Design (LSD)
$\bar{\lambda}$	Slenderness of a compression element
α	Imperfection factor
γ_{M1}	Partial factors for resistance of members
μ	Efficiency factor
ν	Poisson's ratio
χ	Reduction factor for relevant buckling mode
β	Reliability index
ϕ	Resistance factor

determine them. Moreover, no specific criteria exist to determine the effective composite action among CFS profiles connected using batten panels. The EN 1993-1-1 [7] offers design suggestions for limited battened compression members that do not even include the distance between batten panels and the required fasteners to obtain a full composite action.

Recently, a substantial study has been conducted examining the behavior of CFS built-up members [8–27]. Rahnavard et al. [8,9] numerically investigated the effect of the number of fastener rows per batten panel and the optimal distance between the batten panels. Their study was focused on CFS built-up battened columns created by double C-shaped profiles. They also investigated the effect of the geometric shape of the batten panel by comparing a flat batten panel with a U-shaped one. Their results recommended the optimal layout of three rows of fasteners per batten panel. A series of built-up specimens were tested under compression by Dar et al. [10–16] to investigate the spacing effect between individual profiles. The individual lipped channels were arranged back-to-back with specific spacing. They examined the key parameters, such as the maximum load-bearing capacity and failure modes. Their specimens' slenderness covered a suitable range in which the local and global failure modes were seen in their tests. They compared their experimental results with the design approach, including the EN1993-1-3 [5] and the AISI S100 [6], resulting in a more accurate axial load prediction following the EN1993-1-3 [5].

Reyes and Guzmán [17] assessed the impact of the slenderness ratio in CFS built-up box sections by testing 48 experimental specimens. Their CFS built-up columns were created using two C-shaped profiles connected by seam welds with varying spacings. Their results indicated that the modified slenderness provided in the AISI S100 [6] does not necessarily apply to the built-up members with thicknesses of 1.5 and 2 mm and seam weld spacing of less than 600 mm. An experimental and numerical study on the axial behavior of CFS built-up section columns with batten panels was carried out by Dabaon et al. [18–20]. They compared the experimental and numerical results with analytical predictions from available design codes, including the AISI S100 [6], the Australian/New Zealand Standard [21], and the EN 1993-1-3 [5]. Their results showed that the code predictions were unconservative for those specimens that failed by local mode, while for those that failed by global mode, a conservative prediction was achieved.

El Aghoury et al. [22–24] studied the axial behavior of CFS built-up battened columns under concentric and eccentric axial loads. They tested battened columns where four CFS angles were fastened using batten panels. They compared their failure load obtained from the tests and simulation with analytical prediction according to the EN1993-1-3 [5], resulting in the accuracy of the EN1993-1-3 [5] design procedure. Moreover, their results indicated that the design procedure might have errors when the failure mode is due to the interaction of local and global buckling modes. However, the design predictions are unsafe for the column with medium slenderness when the interaction between individual members characterizes the failure modes. A series of experimental tests and numerical analyses were carried out by Anbarasu et al. [25], focusing on CFS built-up battened columns made of lipped angles. They compared the maximum load-bearing capacity obtained from the tested specimens and numerical models with the analytical

prediction following the Australian/New Zealand Standard [21] and the EN1993-1-3 [5]. According to EN1993-1-3 [5], the predictions were safe only for the relatively long CFS built-up battened columns, while unsafe predictions were for the relatively short ones.

Fratamico et al. [26,27] tested sixteen CFS built-up columns with different back-to-back lipped channels. Their results showed that the composite action was achieved most likely when more isolated global buckling occurred. Moreover, their results indicated a higher load-bearing capacity using more fasteners connecting the lipped channel's webs. Zhang and Young [28–31] evaluated the CFS built-up columns using tests and simulations in which the CFS profiles with web stiffeners were used. They compared the maximum load-bearing capacity with the analytical prediction from the AISI S100 [6] and the Australian/New Zealand Standard [21], resulting in the excellent applicability of the AISI S100 [6]. The applicability of the AISI S100 [6] for different types of CFS profiles was investigated in large sets of parametric studies [32–36]. A comprehensive study was conducted by Rasmussen et al. [37], which discussed the composite action of built-up CFS components. They considered the effect of the fasteners' location and effective flexural rigidity to explain the composite action between the individual profiles. Other CFS built-up columns, including built-up Double-Z members, were also investigated using experimental and numerical models [38–56].

Although some studies were performed recently on CFS built-up battened columns, their behavior still needs to be explored more. Additional research related to the design of CFS built-up battened sections is essential to understand their behavior better and develop the design procedures. Moreover, further investigations are necessary to determine the optimal layout to achieve composite action among CFS profiles. This study evaluates the CFS built-up battened columns (two Σ-shaped) under axial compression. An extensive set of finite element models were simulated using the Abaqus [57]. Seventeen experimental specimens of CFS built-up battened columns were selected from the literature to validate the numerical models. The optimal number of fasteners per batten panel and the distance between the batten panels were determined using static displacement control analysis on 100 models. Then, 600 models with different lengths and spacings using the optimal configuration are presented. The load-bearing capacities of these 600 finite element models are compared with the design predictions according to EN 1993-1-3 [5]. The available design procedures in EN 1993-1-3 [5] are discussed and modified.

2. Description of the research study

2.1. The concept of the present study

This paper aims to present the optimal number of fastener rows and the distances between the batten panel, representing a composite action between the individual CFS Σ-shaped profiles. The built-up battened columns were assembled using two CFS Σ-shaped profiles connected using batten panels. The batten panels are fastened to the flanges of the CFS Σ-shaped profiles. The optimal number of the fastener rows per batten panel to reach a composite action between two CFS profiles is unclear. Therefore, the effect of the number of fasteners rows was considered by examining 1 row to 6 rows of fasteners per batten, as shown in Fig. 1. These CFS Σ-shaped profiles can be positioned at various spacings; as a result, different geometries and load-bearing capacities depending on the design requirement, can be achieved. This study covers different profile spacings by considering five h/b ratios as 1.75, 1.50, 1.25, 1.00, and 0.75 (See Fig. 2). These attached batten panels are spaced differently throughout the column's length to obtain the optimal distance between the batten panels. The EN1993-1-1 [7] recommends $15i_{min}$ and $70i_{min}$ for limited CFS built-up configurations, where i_{min} is the minimum radius of gyration of an individual CFS profile. However, the optimal distance between the batten panels still is unclear for the built-up battened column to achieve composite action. This study investigates the batten panels with a distance of (d_{bp}) $15i_{min}$, $30i_{min}$, $45i_{min}$, and $70i_{min}$ to address the mentioned limitation.

2.2. The geometry details

This paper presents a numerical study on the composite action of CFS built-up battened columns. 12 Σ-shaped CFS profiles were considered for this study to cover a broader range of available profile sizes and, consequently, wider slenderness. The geometry details of individual CFS profiles are shown in Fig. 3. Each built-up battened column includes two CFS Σ-shaped profiles, in which the profiles are connected using the batten panels along the length of the column. The batten panels are fastened to both Σ-shaped profile flanges, as indicated in Fig. 4. Self-drilling screws were considered with a diameter (d) of 6.3 mm and a length of 35 mm. The general demand for the end distance (e_1), edge distance (e_2), and distance between the fasteners (d_f) were defined according to the requirements provided by EN1993-1-3 [5]. According to EN 1993-1-3 [5], the end distance from the center of the fastener to the adjacent end of the batten panel, in the direction of load transfer and distance between the fasteners (d_f) should be greater than three times the fastener hole ($e_1 \geq 3d$ and $d_f \geq 3d$). Moreover, the edge distance from the center of the fastener to the adjacent end of the batten panel, perpendicular to the direction of load transfer, should be greater than 1.5 times the fastener hole ($e_2 \geq 1.5d$). As shown in Fig. 4, the distance between the fasteners (d_f) was 20 mm for all models. The end distance from the center of the fastener to the adjacent end of the batten panel was considered 25 mm and 21.5 mm in the direction of load transfer (e_1) and perpendicular to the direction of load transfer (e_2).

Different column lengths, including 2000 mm, 3000 mm, 4000 mm, 5000 mm, and 6000 mm, were considered for each CFS built-up battened column. Two boundary conditions, including pinned and fixed, were investigated in this study. Table 1 lists the information on the models utilized in this study, including their identifying codes.

2.3. Numerical modeling

2.3.1. Material properties

S280GD+Z steel was utilized in this work for both CFS Σ-shaped profiles and batten panels. This study considered the mechanical characteristics of S280GD+Z steel conducted by Craviero et al. [58–61]. The stress–strain curve obtained from tensile coupon testing on S280GD+Z steel [58–61] is shown in Fig. 5. The CFS material was defined using the Abaqus elastoplastic model [57]. Young's modulus and Poisson's ratio are required to model steel materials' elastic characteristics. According to the tensile coupon test [58–61], Young's modulus was 204 GPa. Poisson's ratio was assumed to be 0.3. The plastic behavior was defined using a true stress–strain curve. The true stress–strain curve was converted using the plastic range of the engineering stress–strain curve (Fig. 5). Note that isotropic hardening was chosen to determine the plastic's characteristics. According to the tensile coupon test [58–61], the proportional stress limit was 212.5 MPa. Moreover, the yield stress was 306.81 MPa. The ultimate stress and associated strains were 424.04 MPa and 20%, respectively.

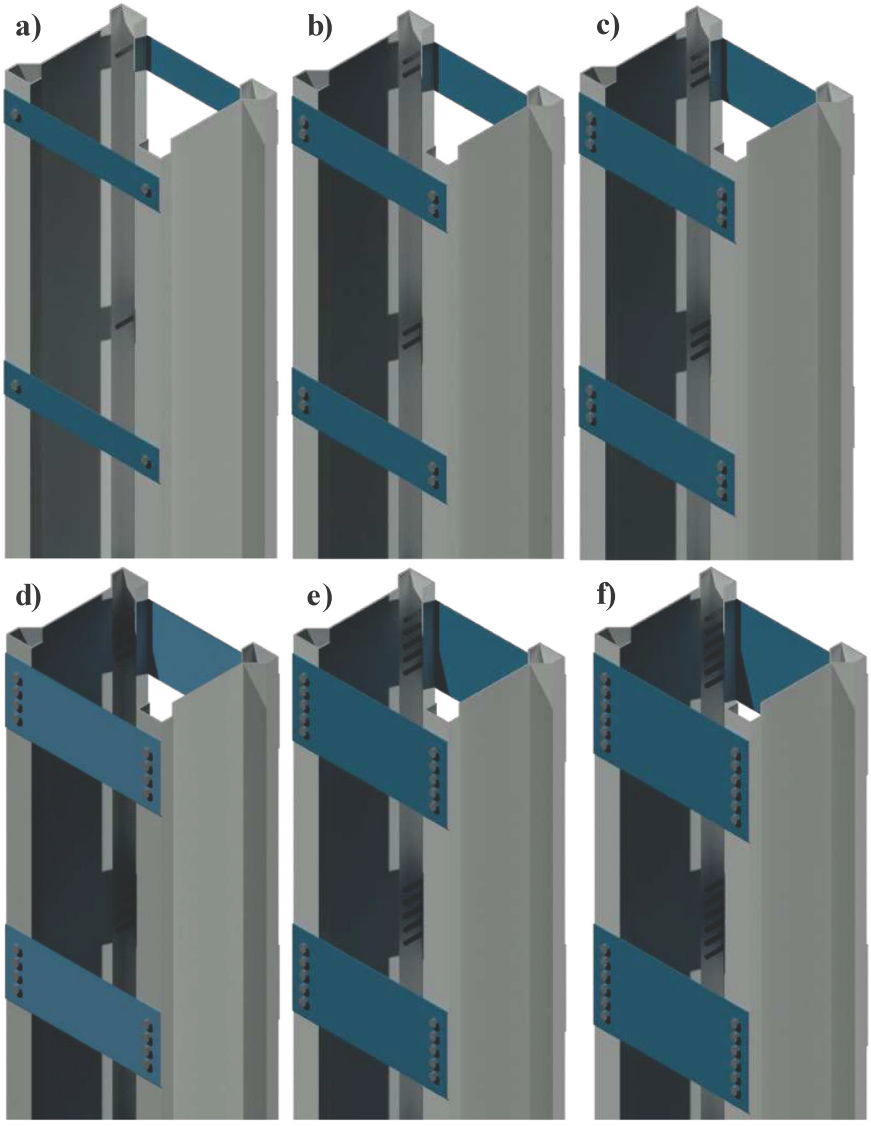

Fig. 1. Example of a battened column with ($h/b = 0.75$) and various fasteners rows per batten panel. **(a)** one row, **(b)** two rows, **(c)** three rows, **(d)** four rows, **(e)** five rows, and **(f)** six rows.

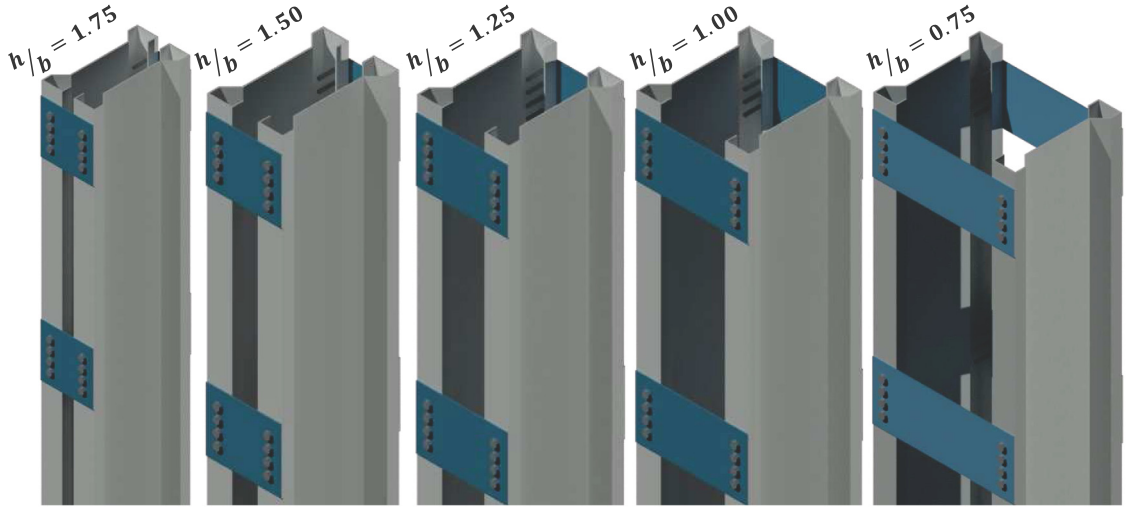

Fig. 2. The battened columns with varied h/b ratio.

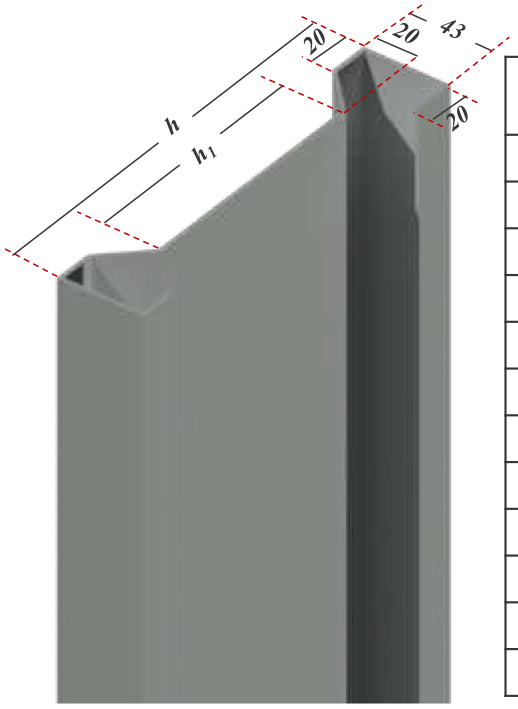

Σ	h (mm)	h_1 (mm)	t (mm)
150×43×2	150	110	2
150×43×2.5	150	110	2.5
150×43×3	150	110	3
170×43×1.5	170	130	1.5
170×43×2	170	130	2
170×43×3	170	130	3
200×43×1.5	200	160	1.5
200×43×2	200	160	2
200×43×3	200	160	3
220×43×1.5	220	180	1.5
220×43×2	220	180	2
220×43×3	220	180	3

Fig. 3. Geometry details of individual CFS profiles.

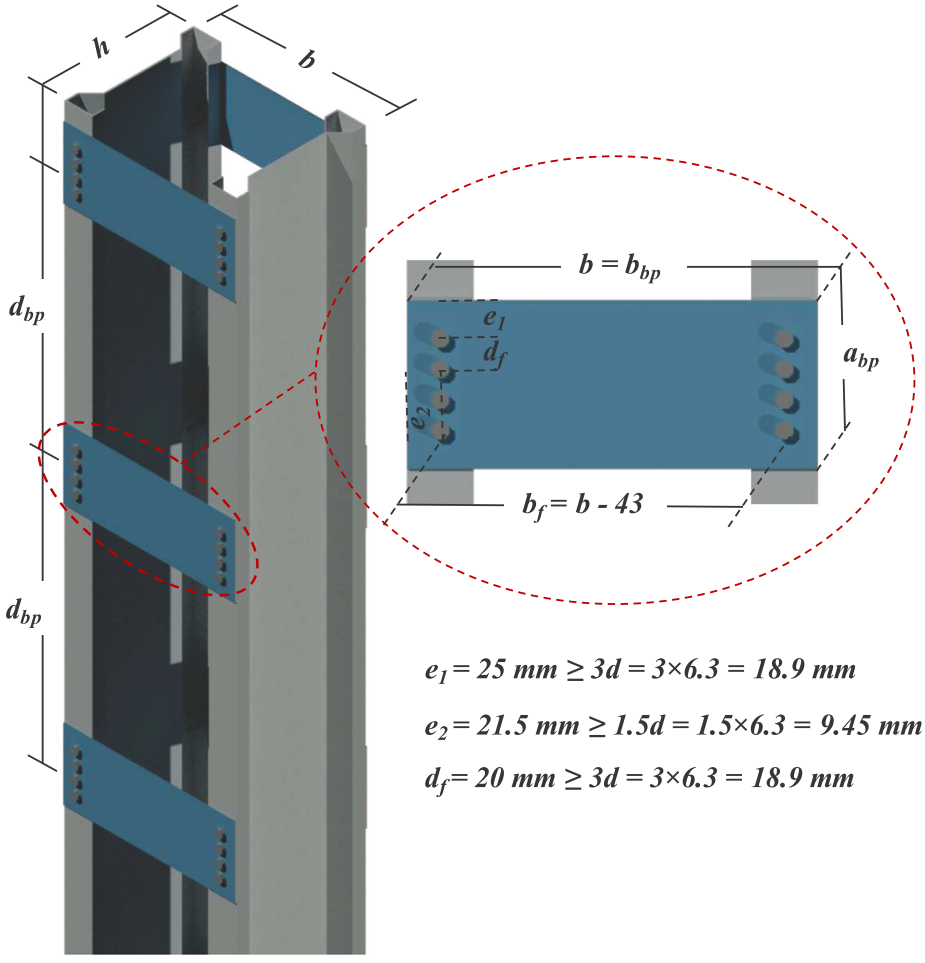

Fig. 4. Geometric details of the battened column.

Table 1
The finite element models.

Models series	Number of models	Column length, L (mm)	Batten panel distance, d_{bp} (i_{min})	Batten panel thickness (mm)	h/b	Number of fasteners rows
2Σ150 × 43 × 2	50	2000 to 6000	30	2	1.75, 1.50, 1.25, 1.00, and 0.75	4
2Σ150 × 43 × 2.5	50	2000 to 6000	30	2	1.75, 1.50, 1.25, 1.00, and 0.75	4
2Σ150 × 43 × 3	50	2000 to 6000	30	2	1.75, 1.50, 1.25, 1.00, and 0.75	4
2Σ170 × 43 × 1.5	50	2000 to 6000	30	2	1.75, 1.50, 1.25, 1.00, and 0.75	4
2Σ170 × 43 × 2	50	2000 to 6000	30	2	1.75, 1.50, 1.25, 1.00, and 0.75	4
2Σ170 × 43 × 3	50	2000 to 6000	30	2	1.75, 1.50, 1.25, 1.00, and 0.75	4
2Σ200 × 43 × 1.5	50	2000 to 6000	30	2	1.75, 1.50, 1.25, 1.00, and 0.75	4
2Σ200 × 43 × 2	150	2000 to 6000	15, 30, 45, 70	2	1.75, 1.50, 1.25, 1.00, and 0.75	1, 2, 3, 4, 5, and 6
2Σ200 × 43 × 3	50	2000 to 6000	30	2	1.75, 1.50, 1.25, 1.00, and 0.75	4
Σ220 × 43 × 1.5	50	2000 to 6000	30	2	1.75, 1.50, 1.25, 1.00, and 0.75	4
Σ220 × 43 × 2	50	2000 to 6000	30	2	1.75, 1.50, 1.25, 1.00, and 0.75	4
Σ220 × 43 × 3	50	2000 to 6000	30	2	1.75, 1.50, 1.25, 1.00, and 0.75	4

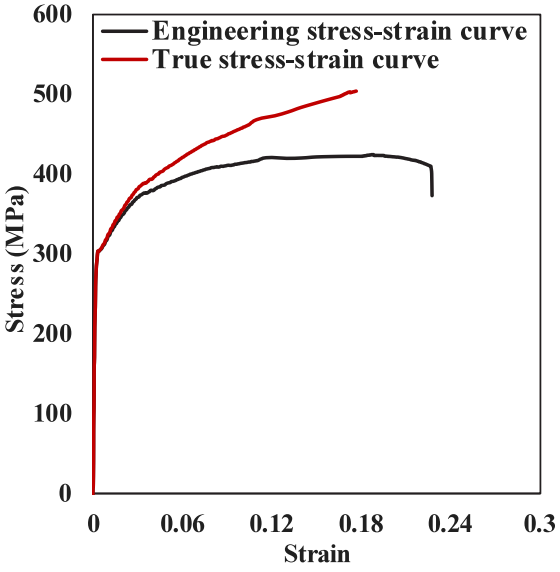

Fig. 5. Stress–strain diagram of the S280GD+Z [58–60].

2.3.2. Interactions and meshing

Proper interactions to specify the contact between batten panels and profiles are critical parameters for successful numerical modeling. The surface-to-surface interaction was selected for defining the interaction among all parts. Contact properties were defined, including normal (hard contact) and tangential (coefficient of 0.2).

Three modeling techniques were employed to model the self-drilled fasteners:

- A combination of beam connectors and fasteners: the beam connector specifies the connection between two nodes on two surfaces in this approach. From one surface to another, the "fastener" tool attached the actual radius of the fasteners to the beam connection. Fig. 6 illustrates a combined "beam connector and fastener".
- Modeling the actual self-drilled fasteners using solid elements: for this modeling technique, the elastic and plastic material property was defined according to the stress–strain curve presented for self-drilling [62,63].
- A combination of Cartesian connector and fastener: the Cartesian connector specifies the connection between two nodes on two surfaces in this approach. In this modeling approach, the shear stiffness of the self-drilled fastener was defined according to the experimental tests conducted by Huynh et al. [62].

2.3.3. Imperfection, boundary conditions, and loading

Fig. 6 shows the details of boundary conditions and loading. Two reference points, RP-1 and RP-2, were coupled to the column ends. Two boundary conditions, including pinned and fixed, were considered in this study. As is shown in Fig. 6, only three transitional directions (U_x, U_y, and U_z) were restrained from defining the pinned boundary condition. The transitional direction (U_x, U_y, and U_z) and the rotational movements (θ_x, θ_y, and θ_z) were also blocked to define the fixed boundary condition. However, it should be mentioned that one of the reference points (RP-2) was free to move transitionally in the longitudinal direction to be axially loaded. No relative movement between the individual elements of the built-up member could occur because both column ends were coupled to the reference points.

Linear buckling analysis and nonlinear general static analysis available in the Abaqus [57] were used in this study. The linear buckling analysis was undertaken to obtain the buckling mode shapes. These buckling mode shapes were used to define the initial imperfection for the CFS profiles. A combination of local and flexural buckling modes was proposed to determine the initial imperfection. Previous research studies suggested the imperfection amplitude of 1/1000 of the column length for global buckling mode. Craveiro et al. [60] proposed a value of 1/200 of the section height as amplitude for the local buckling mode. However, the readers should be aware that EN 1993-1-1 [7], clause 6.4.3, recommended L/500 for the battened columns.

Moreover, a sensitivity analysis was performed by Rahnavard et al. [8,9] that showed an accuracy of axial load prediction by selecting 1/1000 of the column length for the global buckling mode and 1/200 of the section height as amplitude for the local buckling mode. Fig. 7 shows examples of selected buckling modes for the 2Σ200 × 43 × 2 model. The defined initial geometric imperfection modes depicted in Fig. 7 include global buckling (Fig. 7-**a**) and local buckling (Fig. 7-**b**).

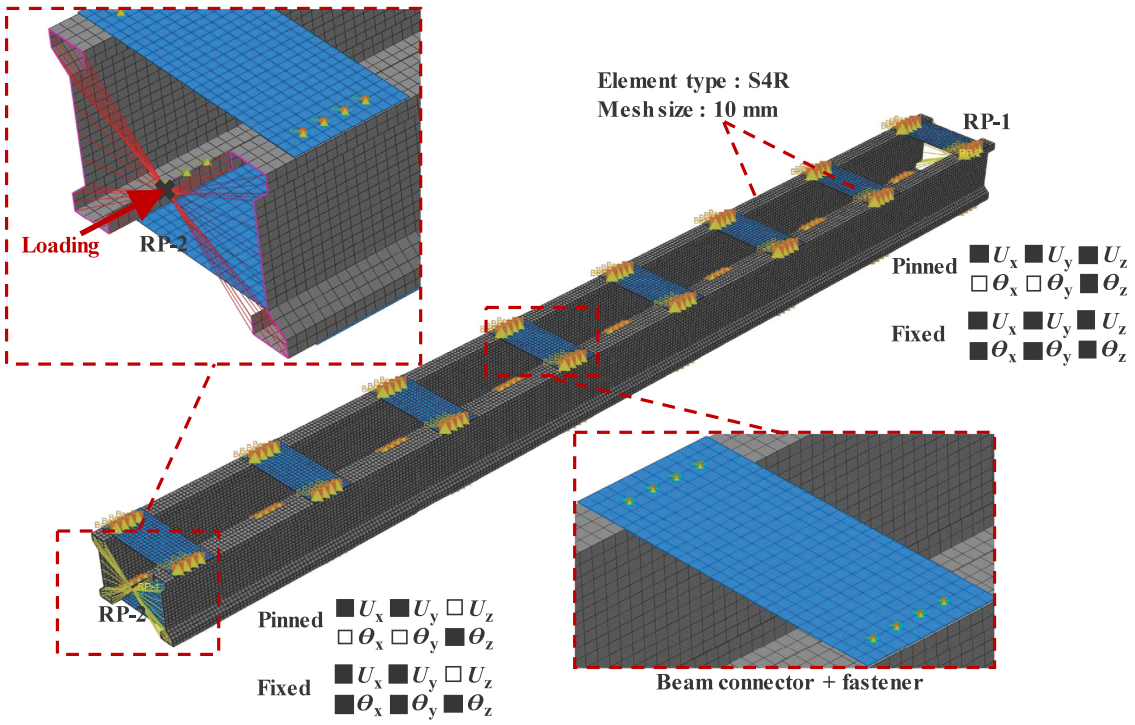

Fig. 6. Finite element modeling.

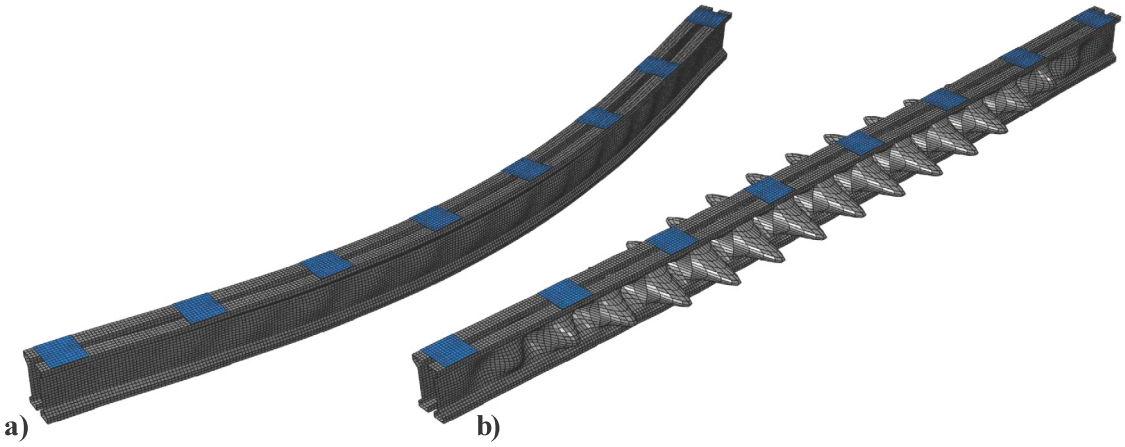

Fig. 7. The used buckling modes as initial imperfection; **(a)** global and **(b)** Local.

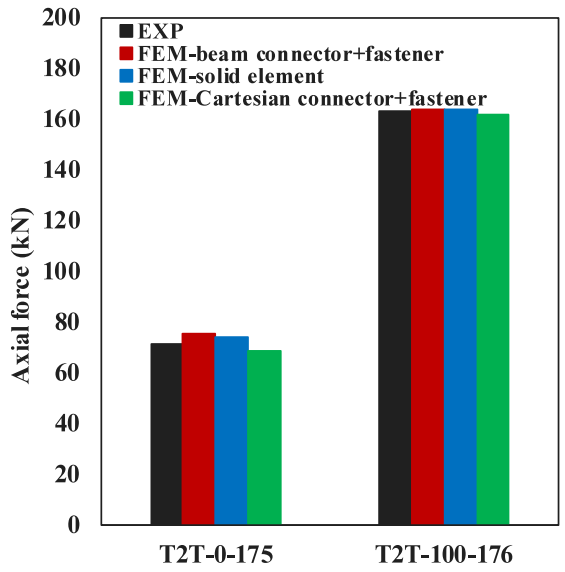

Fig. 8. Axial force for experimental tests [10] and numerical modeling with different modeling approaches.

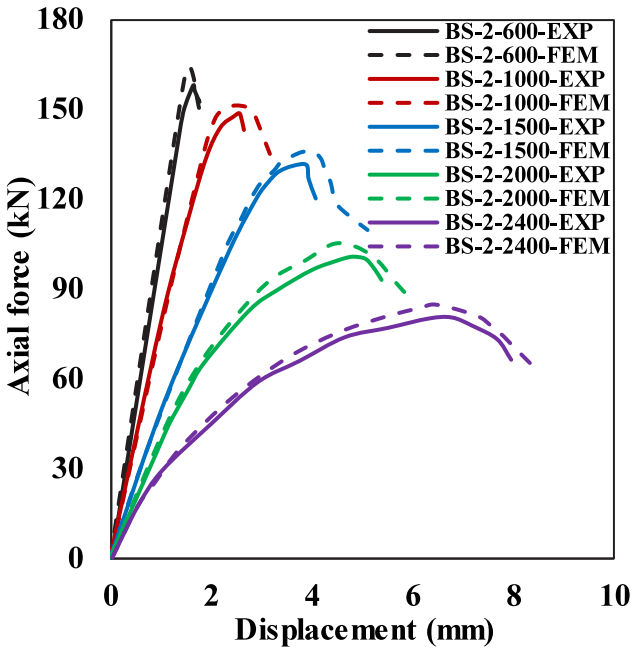

Fig. 9. Force vs. shortening displacement curves for experimental specimens [11] and numerical models.

2.3.4. Finite element modeling validation

In this section, previous studies' experimental tests were selected and modeled using the mentioned techniques in Section 2. Two CFS built-up battened columns (T2T-0-175 and T2T-100-175) were selected from the experimental work conducted by Dar et al. [10] to compare the modeling techniques used for self-drilled fasteners. Two U-shaped CFS profiles were connected in the experimental specimens by employing batten panels of 6 mm thickness and 5 mm diameter self-drilling screws. The U-shaped CFS profiles had a web depth of 100 mm, a flange width of 25 mm, and a thickness of 2 mm. The distance between the batten panels along the columns was 175 mm. Moreover, The spacing between the U-shaped CFS was 0 mm and 100 mm for T2T-0-175 and T2T-100-175, respectively.

Fig. 8 compares the axial load-bearing capacity obtained from the experimental tests [10] and numerical models with different modeling approaches. For the case of T2T-0-175, the axial load-bearing capacity obtained from the experimental test was 71.5 kN. The numerical results showed 75.5 kN, 74.2 kN, and 68.58 kN for "beam connector+fastener", solid element, and "beam connector+fastener", respectively. By comparing the results for T2T-0-175, it can be seen that all modeling approaches predicted the experimental results well. A similar conclusion was obtained for the case of T2T-0-175. The axial load-bearing capacity obtained from the experimental test was 163.01 kN. The numerical results showed 164.13 kN, 163.98 kN, and 161.94 kN for "beam connector+fastener", solid element, and "beam connector+fastener", respectively. Therefore, it can be concluded that the simplified connector+fastener technique can represent the self-drilling fastener behavior as accurately as the actual solid element. In addition, modeling the actual fastener using solid elements required much computational calculation and was a time-consuming modeling approach. Consequently, the simplified connector+fastener technique was used in the following.

Additional experimental tests were selected and modeled using the mentioned "beam connector+fastener" techniques. Five CFS battened column specimens with various lengths from a research study conducted by Dar et al. [11] were modeled. The selected CFS built-up battened column specimens were with a lengths of 600 mm (BS-2-600), 1000 mm (BS-2-1000), 1500 mm (BS-2-1500), 2000 mm (BS-2-2000), and 2400 mm (BS-2-2400). The axial force vs. vertical displacement curves obtained from the finite element models and experimental specimens were compared (Fig. 9). As shown in Fig. 9, the finite element models predicted the axial capacity of the experimental CFS built-up battened columns.

Two more built-up CFS experimental column specimens [61] with rectangular (R-2Σ+2U) and square (S-2Σ+2U) section shapes were considered to verify the numerical models employed in this work. The experimental CFS built-up column specimens were built using CFS Σ-shaped and U-shaped with a thickness of 1.5 mm. The length of the selected CFS built-up column specimens was 1050 mm. More information about the experimental specimens is available in [61]. Fig. 10 compares the experimental and numerical results for the rectangular CFS built-up column in load-bearing capacity and buckling deformations. Very similar load-bearing capacity and deformation can be seen, indicating excellent agreement between experimental and numerical results. A similar conclusion can be made for the square CFS built-up column, as shown in Fig. 11.

Ten more built-up CFS experimental column specimens composed of two Σ-shaped CFS profiles [30] were considered to investigate the reliability of the modeling techniques used in this paper. The experimental CFS built-up box column specimens were built using two CFS with edge and web stiffeners. Two thicknesses, including 0.48 mm and 1.00 mm, were considered according to the experimental study by Zhang et al. [30]. Different lengths were selected for CFS built-up box columns, including 300 mm, 800 mm, 1400 mm, 2000 mm, and 3200 mm. More information about the experimental specimens is available in [30]. A comparison of the maximum axial load obtained from experimental specimens and numerical models is listed in Table 2. The experimental tests [24] and the numerical models showed a similar load-bearing capacity, indicating excellent agreement between experimental and numerical results ($\leq$7%). These close agreements show that presented finite element modeling techniques can be reliable for performing this parametric study.

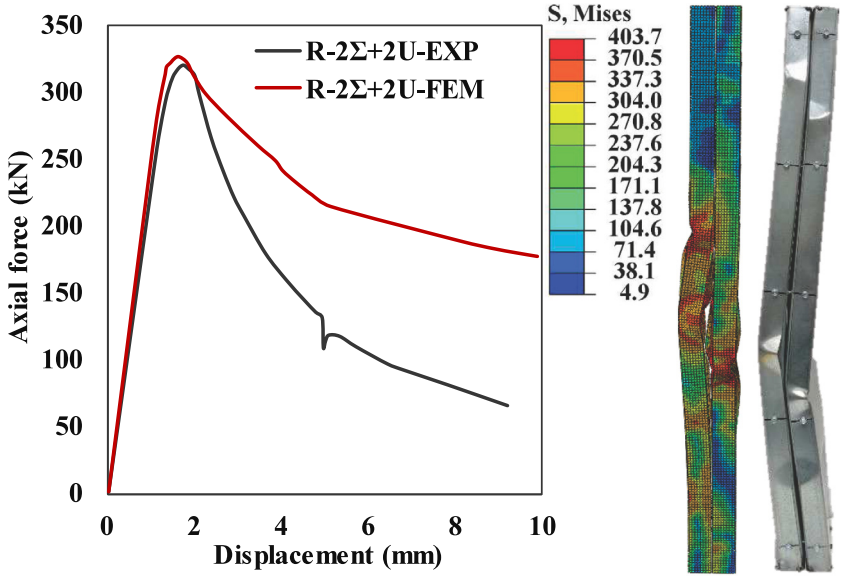

Fig. 10. Comparison of the experimental [61] and numerical results for rectangular built-up Σ-shaped.

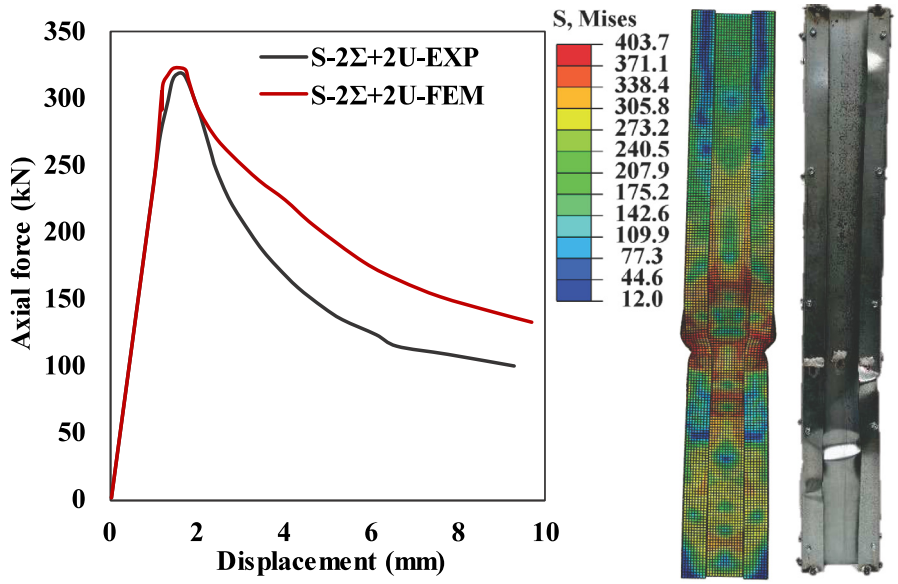

Fig. 11. Comparison of the experimental [61] and numerical results for square built-up Σ-shaped.

Table 2
Comparison of the test [30] and modeling axial capacities.

Specimen ID	Axial load-bearing capacity (kN)		FEM/EXP	Specimen ID	Axial load-bearing capacity (kN)		FEM/EXP
	EXP	FEM					
VT0.48L300	43.30	45.2	1.04	VT1.0L300	137.6	138.19	1.00
VT0.48L800	41.20	43.05	1.04	VT1.0L800	135.2	131.47	0.97
VT0.48L1400	39.50	41.75	1.06	VT1.0L1400	129.8	123.82	0.95
VT0.48L2000	37.70	39.15	1.03	VT1.0L2000	127.9	119.95	0.93
VT0.48L3200	31.70	34.05	1.07	VT1.0L3200	81.9	79.15	0.97
Mean value			1.04	Mean value			0.96
Standard deviation			0.01	Standard deviation			0.02

3. Results and discussion

3.1. The optimal number of fasteners per batten panels

The effect number of fastener rows is investigated in this section. For this purpose, the force versus displacement curve for CFS built-up battened columns with a different number of fastener rows varying from one row to six rows were compared in Figs. 12 and 13. The CFS built-up battened column of 2Σ200 × 43 × 2 with a length of 3000 mm was chosen for this comparison. The distance between batten panels was considered *L/4* for models. Although the axial load-bearing capacity analysis was performed for all *h/b* ratios (Fig. 2), this section presents the axial force–displacement curve for the models with $h/b = 0.75$ and 1.75, and the maximum capacity of the other models was compared in Fig. 14. As seen for the battened column with both fixed ends (Fig. 12**a**) and pinned end (Fig. 12**b**) for $h/b = 0.75$, the axial load-bearing capacity increased by increasing the number of fastener rows. As shown in Fig. 12**a**, when the number of fasteners rows of the battened column with fixed ends increased from one to four, the load-bearing capacity increased from 255.28 kN to 294.97 kN, indicating that the axial capacity improved by 15%. However, the increase in axial load-bearing capacity is negligible (less than 4%) when the fasteners row per batten panel rises from four to five and six. A similar comparison for the pinned battened column is visible in Fig. 12**b**. When the *h/b* ratio was 1.75, as shown in Fig. 13, the axial load-bearing capacity of the battened column with fixed ends (Fig. 13**a**) and pinned ends (Fig. 13**b**) increased with the number of rows of fasteners. Fig. 13**a** demonstrated a 14% improvement in axial capacity when the number of fastener rows in a battened column with fixed ends was increased from one to four. However, going from four to five or six fasteners per batten panel only results in a little boost in axial load-bearing capacity. Comparing Figs. 12 and 13 shows that the differences between the capacity of the fixed and pinned battened columns are remarkable when the *h/b* ratio was 1.75, while for $h/b = 0.75$, this difference was ignorable, resulting in less composite action between CFS profiles when their spacing increased.

A summary of the maximum axial load of the battened column with different *h/b* ratios is shown in Fig. 14 to investigate the effect

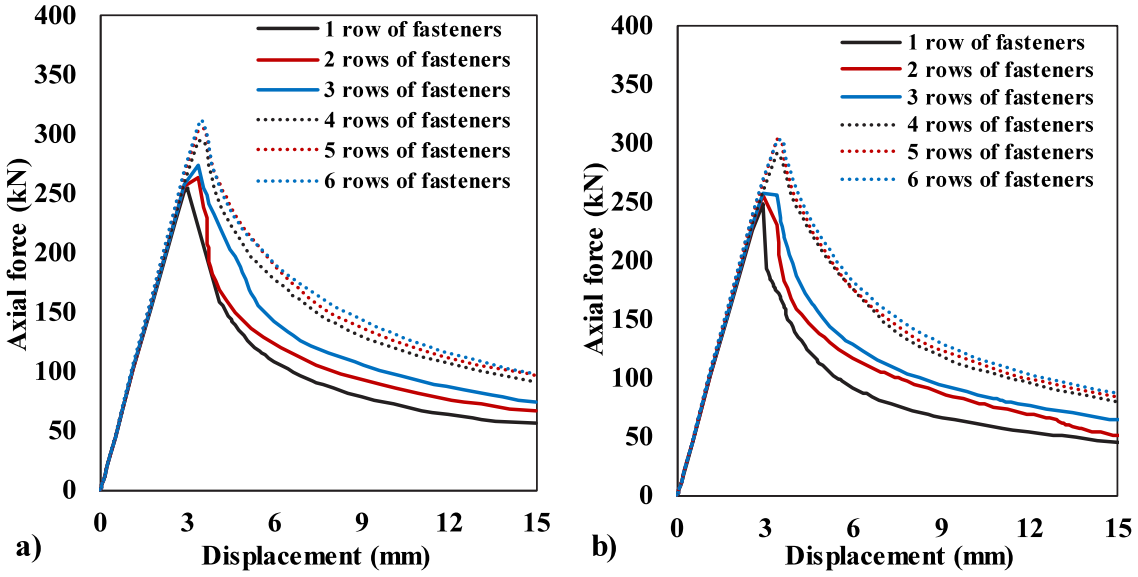

Fig. 12. Force–shortening displacement curves for a battened column with $h/b = 0.75$ and the different number of fastener rows per plate; **(a)** fixed ends and **(b)** pinned ends.

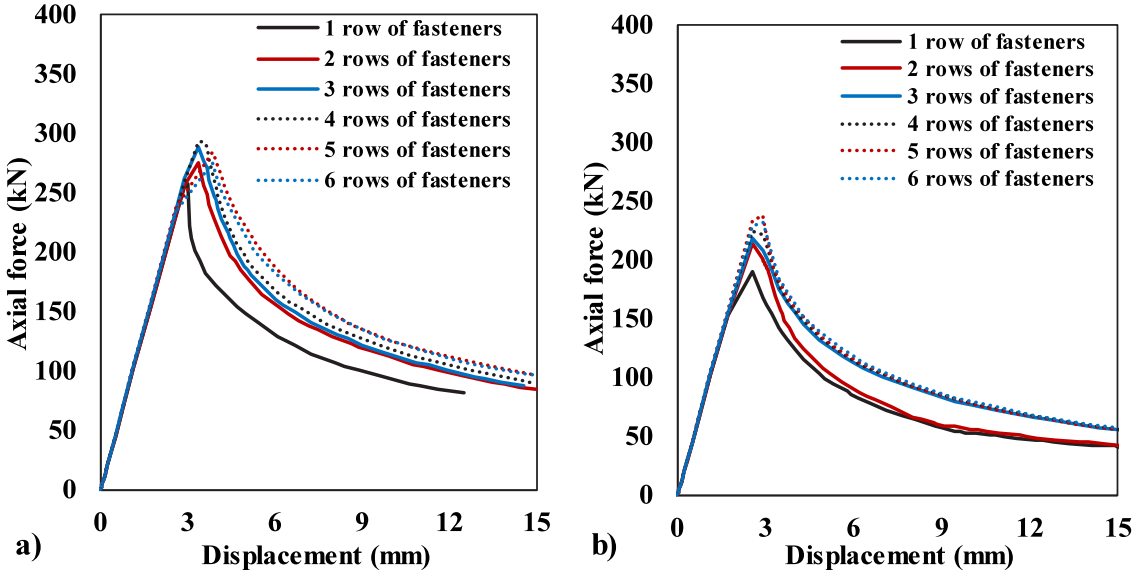

Fig. 13. Force–shortening displacement curves for a battened column with $h/b = 1.75$ and the different number of fastener rows per plate; **(a)** fixed ends and **(b)** pinned ends.

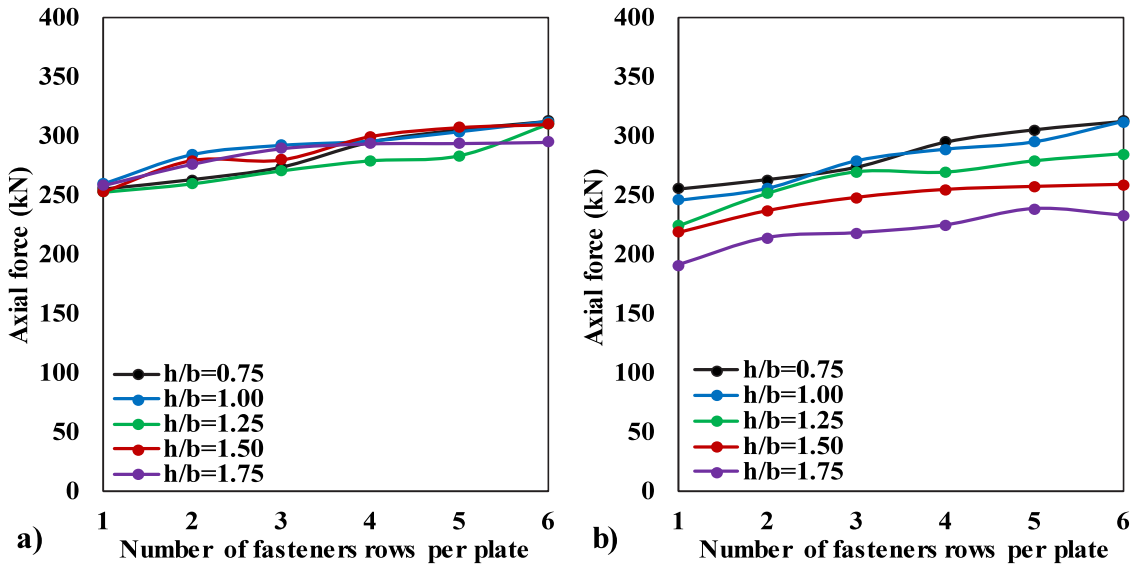

Fig. 14. The effect of the number of fastener rows per batten panel; **(a)** fixed ends and **(b)** pinned ends.

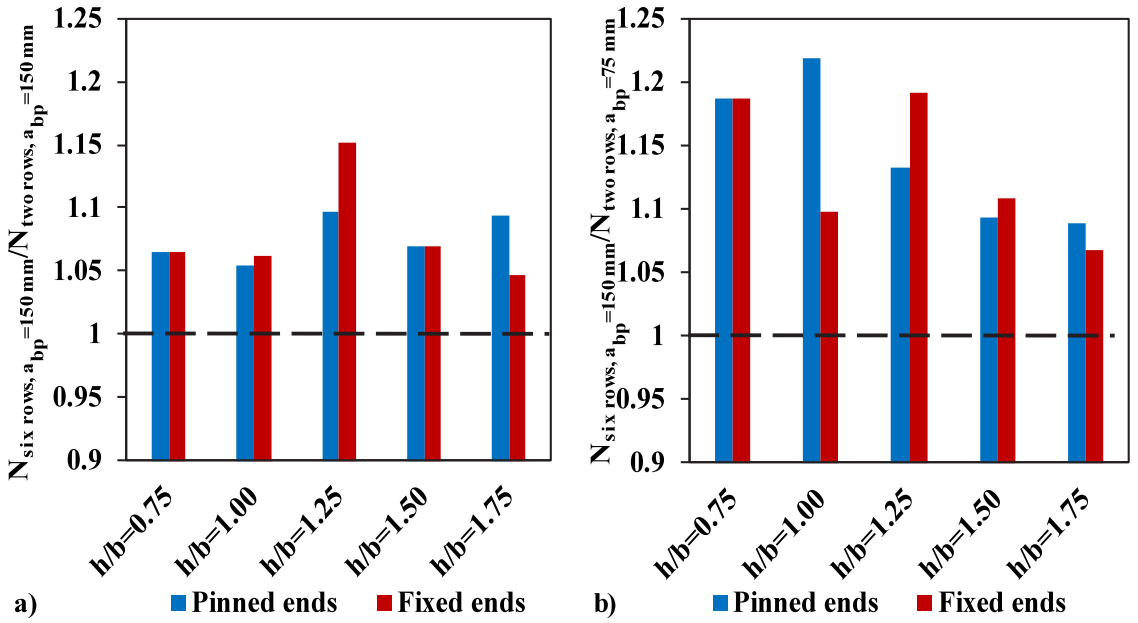

Fig. 15. The effect of the number of fastener rows with **(a)** the same batten panel dimension and **(b)** different batten panel dimensions.

of the number of fastener rows for more cases of the battened column geometry. The *h/b* ratios are explained in Fig. 2 and Table 1. Both fixed and pinned boundary conditions were evaluated. This comparison is for the CFS built-up battened column of 2Σ200 × 43 × 2 with a length of 3000 mm and batten panel distance of L/4 (725 mm). As can be seen, by increasing the number of fastener rows up to four per batten panel, the load-bearing capacity increased remarkably; however, with more than four rows of fasteners, the axial load improvement is ignorable. Therefore, the four rows of fasteners were selected as the optimal number of fasteners. This study suggests that the more fastener rows there are, the closer the composite action's behavior is to be detected. It is worth mentioning that the previous study [4] for CFS built-up sections with different profile shapes (C-shaped profiles) suggested the battened column with three rows of fasteners per batten panel as the optimal layout.

It should be noted that the shear forces of the fasteners were always less than the shear strength of the self-drilled fasteners (12 kN, according to [62]). Furthermore, for the chosen experimental tests, there were no significant shear deformations along the columns' length or boundary conditions [30,61]. In addition, no significant shear deformation was reported in the experimental built-up columns with battened panels [10,11]. Moreover, this study's simulation of the boundary condition involved coupling each column end to a reference point (RF1 and RF2). Since this is the case, the nodes at the column ends must move simultaneously. At the boundary conditions of the profiles, there are no relative deformations (shear deformations). For the same reason, batten panels close to the column end (50 mm) were used to avoid shear deformations.

It should be noted that the width of the battens was increased to facilitate the inclusion of a larger number of fasteners. Therefore, a more detailed study was performed to discuss further the effect of increasing the batten's stiffness and the number of fasteners. For this purpose, the CFS built-up battened column of 2Σ200 × 43 × 2 with a length of 3000 mm was chosen for this comparison. The distance between batten panels was considered *L/4* for models. Fig. 15**a** shows the axial load ratio for battened columns when the number of rows of

fasteners increases from 2 to 6, and the plate width (a_{bp} in Fig. 4) was considered 150 mm. Similarly, Fig. 15**b** shows the axial load ratio for battened columns when the number of fasteners rows increases from 2 to 6, and the plate width increases from 75 mm to 150 mm to facilitate the inclusion of a more significant number of fasteners.

As shown in Fig. 15**a**, by increasing the number of fastener rows and keeping the batten panel width (a_{bp}) the same, the axial capacity of the battened columns was increased. However, the axial capacity of the battened columns was increased more significantly when the number of fastener rows and the width of the batten panels were increased (Fig. 15**b**). Therefore, it is concluded that increasing the axial load-bearing capacity due to the number of fasteners also affected the batten panel's stiffness.

3.2. The optimal batten panels distance

The axial force vs. displacement curves for battened CFS built-up columns with various batten panel distances are depicted in Figs. 16 and 17. Note that the column length is 3000 mm, and the h/b is 0.75 and 1.75. Four rows of fasteners per batten panel were used, aiming to make a composite action between two $\Sigma 200 \times 43 \times 2$ profiles. The batten panels' distances vary by $15i_{min}$, $30i_{min}$, $45i_{min}$, and $70i_{min}$. For the case of the battened columns with h/b of 0.75 and fixed ends (Fig. 16**a**), when the batten panel distance is $70i_{min,}$ the capacity is 254.34 kN. By decreasing the distance to $30i_{min}$, the axial capacity increases to 339.17 kN, showing a 33.3% enhancement. However, by reducing the distance by 50% ($15i_{min}$), the axial capacity increases only 1.5%. Similarly, for the battened column with h/b of 0.75 and pinned ends (Fig. 16**b**), the decreasing distance between batten panels up to $30i_{min}$ increases the axial bearing capacity significantly. More reduction of batten panel distance than $30i_{min}$ slightly affects the axial behavior.

For the case of the battened columns with h/b of 1.75 and fixed ends (Fig. 17**a**), when the batten panel distance is $70i_{min,}$ the capacity is 254.09 kN. By decreasing the distance to $30i_{min}$, the axial capacity increases to 325.01 kN, showing a 27.9% enhancement. However, by reducing the distance by 50% ($15i_{min}$), the axial capacity increases only 0.5%. Similarly, for the battened column with h/b of 0.75 and pinned ends (Fig. 17**b**), the decreasing distance between batten panels up to $30i_{min}$ increases the axial bearing capacity significantly. More reduction of batten panel distance than $30i_{min}$ slightly affects the axial behavior.

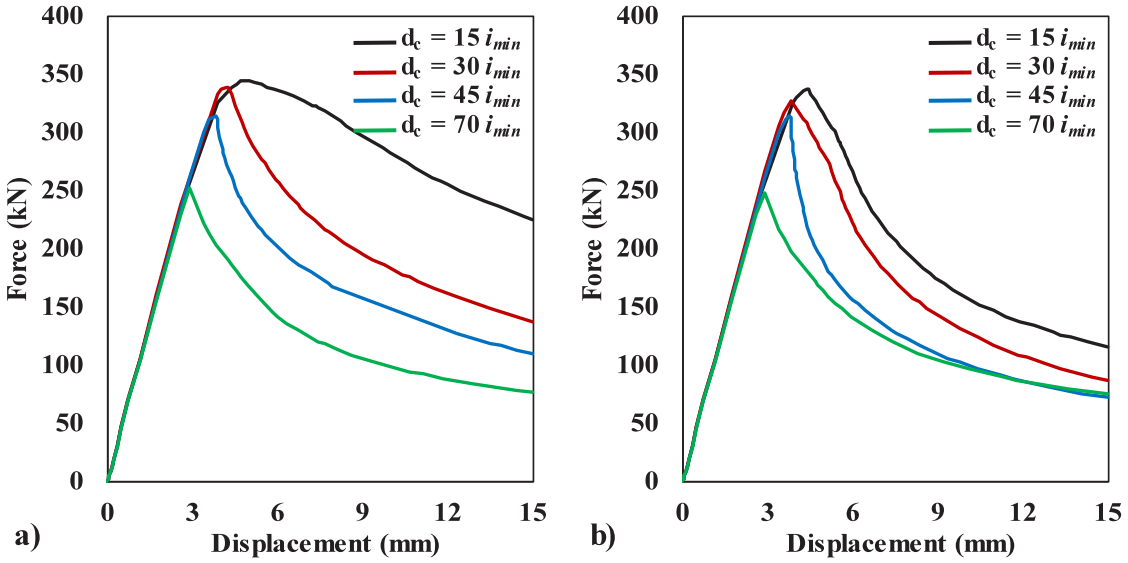

Fig. 16. Axial force vs. displacement curves for the battened column with $h/b = 1.75$ and various batten panel distances **(a)** fixed column ends and **(b)** pinned column ends.

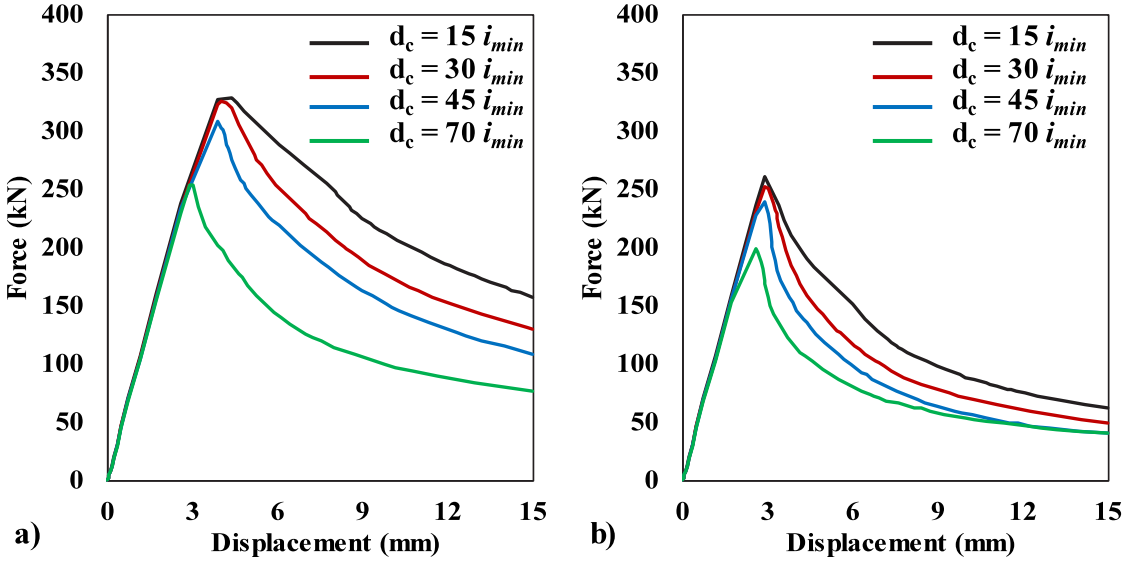

Fig. 17. Axial force vs. displacement curves for the battened column with $h/b = 1.75$ and various batten panel distances **(a)** fixed column ends and **(b)** pinned column ends.

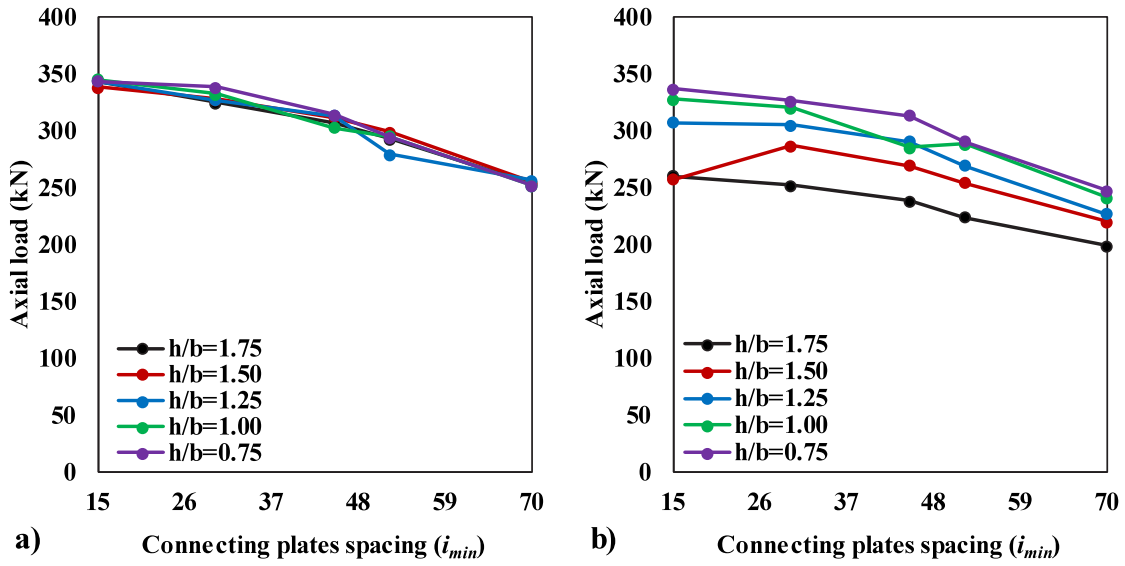

Fig. 18. The effect of the batten panel distance of battened column with: **(a)** fixed ends and **(b)** pinned ends.

Comparing Figs. 16 and 17 shows that the differences between the capacity of the fixed and pinned battened columns are remarkable when the h/b ratio was 1.75, while for $h/b = 0.75$, this difference was ignorable, resulting in less composite action between CFS profiles when their spacing increased.

For more evaluation of the effect of batten panel distance on the compression capacity of battened columns, various h/b ratios following Fig. 2 and Table 1 were analyzed. A comparison of the maximum capacity of battened columns with different h/b ratios and various batten panel distances is shown in Fig. 18. For battened columns with fixed ends (Fig. 18**a**), the axial load-bearing capacity increases by decreasing batten panel distance, showing a significant effect.

Moreover, the batten panel distance considerably impacts the pined battened columns' axial compression capacity (Fig. 18**b**). Therefore, it is concluded that the optimal batten panel distance for the investigated configuration is $30i_{min}$. This finding agrees with the suggestion provided by Rahnavard et al. [8,9] for the battened CFS columns containing two C-shaped profiles.

The EN1993-1-1 [7] specified a maximum distance of $70i_{min}$ and $15i_{min}$ between connectors for various built-up designs. This paper proposed a minimum batten panel distance of $30i_{min}$ and four rows of fasteners per batten panel for CFS built-up column sections to accomplish composite action. Note that this suggestion is only valid for the sections under this investigation. More investigation, including experimental tests and numerical modeling of different geometries and slenderness, is essential to obtain a reliable conclusion for a wider range of cross-sections.

3.3. The effect of the stiffness of the self-drilled fastener

This section discussed the effect of self-drilling stiffness. For this purpose, four different stiffness values ranging from 5.5 kN/mm to 55 kN/mm were considered according to the experimental study conducted by Huynh et al. [62]. The CFS built-up battened column (two $\Sigma 200 \times 43 \times 2$ profiles) with a length of 3000 mm and an h/b ratio of 0.75 was considered. The h/b ratio of 0.75 was selected because the shear force effect for the battened column with larger spacing between CFS profiles (h/b ratio of 0.75) is more considerable than those with h/b ratios of 1.75, 1.50, 1.25, and 1.00. Fig. 19 compares the effect of the stiffness of the self-drilled fasteners for fixed and pinned CFS battened columns. As can be seen, by increasing the stiffness of the self-drilling fasteners, the axial load-bearing capacity increased—however, this increase is remarkable up to a certain level of the self-drilling

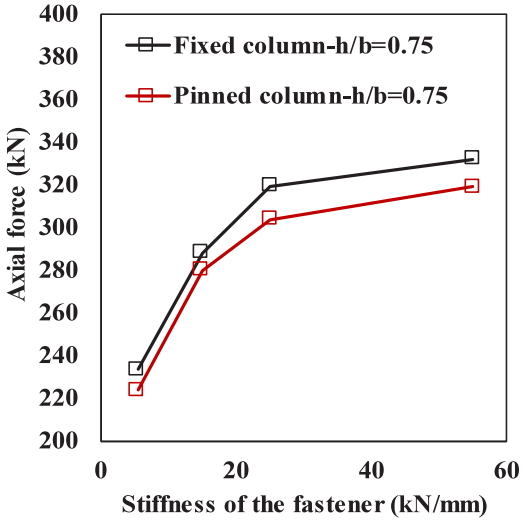

Fig. 19. The effect of the stiffness value on the axial load-bearing capacity.

stiffness. For the fixed column, by increasing the fasteners' stiffness from 5.5 kN/mm to 25 kN/mm, the axial capacity increased from 233.51 kN to 319.47 kN, indicating a 36.8% improvement. However, by increasing the fasteners' stiffness from 25 kN/mm to 55 kN/mm, the axial capacity increased only 0.4%. A similar conclusion can be achieved for the pinned CFS battened columns.

3.4. Failure mode

This section discussed the obtained failure mode for the CFS built-up battened columns. For this purpose, the failure model for the battened column of $2\Sigma 200 \times 43 \times 2$ with the distance between batten panels of $30i_{min}$ was selected as suggested in Section 3.2. The column length of 2000 mm, 3000 mm, 4000 mm, 5000 mm, and 6000 mm was selected. Each batten panel fastened the CFS profiles using four rows of fasteners as recommended in Section 3.1. The h/b ratio of 1.75 with pinned boundary conditions has been considered in this section. Fig. 20 shows the failure mode for each CFS built-up battened column with different lengths.

Flexural and local buckling about the minor axis was the major buckling mode for the CFS battened column with lengths of 2000 mm (see Fig. 20**a**). The buckling deformation at the maximum load results

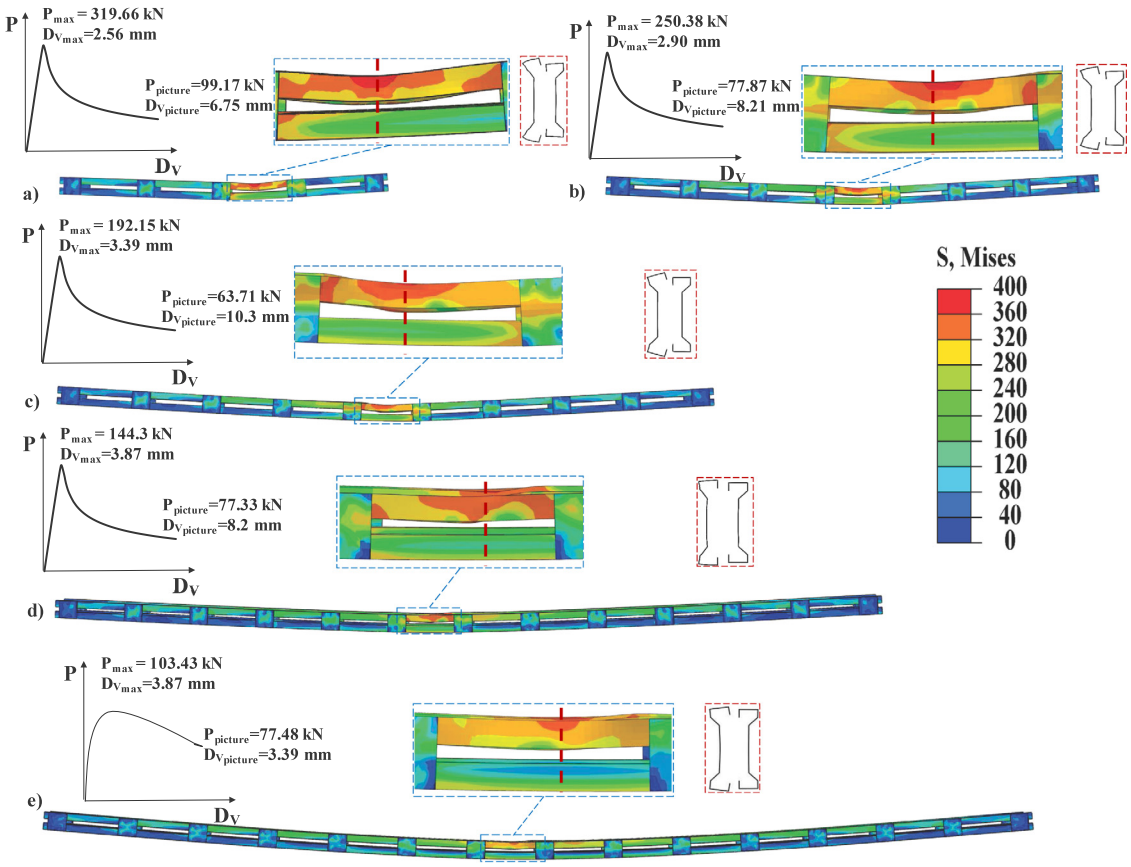

Fig. 20. Failure mode for the CFS built-up battened column with an h/b ratio of 1.75 and a length of **(a)** 2000 mm, **(b)** 3000 mm, **(c)** 4000 mm, **(d)** 5000 mm, and **(e)** 6000 mm.

from the combination of flexural and local deformations. One of the Σ-shaped profiles had its web moved inward, causing a distortional buckling in the flanges.

All other models of CFS battened columns with lengths more than 2000 mm failed due to global flexural buckling about the minor axis (Fig. 20**b–e**). Flexural buckling about the minor axis, positioned between the batten panels at mid-span, is the most common failure mode, as depicted in Fig. 20**b–e**. For the case of the CFS column with a length of 3000 mm, a flexural with a minor local buckling was seen (Fig. 20**b**). There was no evidence of local buckling at the maximum load for the columns with lengths of 4000 mm, 5000 mm, and 6000 mm (Fig. 20**c–e**). However, some local deformations are seen at significant lateral deformations (at the end of loading).

4. Parametric study and analytical approaches

4.1. Parametric study

The optimal distance between batten panels and the number of fastener rows per batten panel for a battened column configuration with double Σ-shaped profiles to have a full or partial composite action was discussed in Section 3. Section 3 suggested the optimal distance between batten panels as $30i_{min}$. Moreover, four rows of fasteners per batten panel were recommended as the optimal number of fasteners rows. This section uses 600 finite element models and compares them with analytical approaches. Twelve battened column sections were selected. All models were in lengths, including 2000 mm, 3000 mm, 4000 mm, 5000 mm, and 6000 mm. The h/b ratios, including 1.75, 1.50, 1.25, 1.00, and 0.75, were also considered to expand the results for a wider range of spacing. The details of the models can be found in Table 1.

4.2. Reliability analysis

Reliability analysis was carried out in this research to compare predictions obtained from different analytical methodologies. Reliability analysis represents the probability of failure. This study evaluated the analytical methods by comparing their reliability index (β) following the AISI S-100 [6]. The reliability index (β) can be obtained from Eq1. The statistical parameters in Eq. (1), including M_m, F_m, V_M, and V_F were assumed as 1.10, 1.00, 0.10, 0.05, respectively [6,58,61]. P_m and V_P are the mean value and the coefficient of variation obtained from the finite element to the design prediction ratios (see Tables 3 to 5). The coefficient of the mean load effect variation (V_Q) was considered 0.21 by adopting the dead load (DL) over live load (LL) as 0.2. The load combination of 1.35DL+1.5LL from Eurocode was selected. The resistance factor (ϕ) of 1.00 [5] also was considered to calculate the ratio $\frac{R_n}{Q_m}$. The correction factor (C_P) was considered for the number of models evaluated in this study. The correction factor (C_P) can be calculated using Eq. (2), where n is the number of the models and m is the degrees of freedom and equal $n-1$. The reliability index of 2.5 was targeted for a reliable analytical prediction.

$$\beta = \frac{\ln(M_m F_m P_m \times \frac{R_n}{Q_m})}{\sqrt{V_M^2 + V_F^2 + C_P V_P^2 + V_Q^2}} \quad (1)$$

$$C_P = (1 + 1/n)(m/m-2) \quad (2)$$

4.3. EN1993-1-1, clause 6.3.1 [1]

The axial load-bearing capacity of the CFS built-up battened columns can be carried out through advanced design calculations such as the finite element and standardized design methods. This section compares the axial load-bearing capacity obtained from finite element

Table 3
Reliability analysis for the analytical prediction based on the EN1993-1-1, clause 6.3.1 [7] formulas.

Cold-formed battened columns	Fixed battened column		Pinned battened column	
	$\frac{N_{FEM}}{N_{b,Rd}}$ (*curve a*)	$\frac{N_{FEM}}{N_{b,Rd}}$ (*curve b*)	$\frac{N_{FEM}}{N_{b,Rd}}$ (*curve a*)	$\frac{N_{FEM}}{N_{b,Rd}}$ (*curve b*)
Number of models #	300	300	300	300
Mean (P_m)	1.08	1.12	1.05	1.13
Standard deviation	0.051	0.054	0.065	0.065
COV (V_P)	0.047	0.048	0.062	0.058
Resistance factor (ϕ)	1.00	1.00	1.00	1.00
Correction factor (C_P)	1.01	1.01	1.01	1.01
Reliability index (β)	2.28	2.42	2.13	2.44

Table 4
Reliability analysis for the analytical prediction based on the EN1993-1-1, clause 6.3.1 [7] formulas incorporated with the recommended slenderness ratio from the AISI S100-16 [6].

Cold-formed battened columns	Fixed battened column		Pinned battened column	
	$\frac{N_{FEM}}{N_{b,Rd}}$ (curve a)	$\frac{N_{FEM}}{N_{b,Rd}}$ (curve b)	$\frac{N_{FEM}}{N_{b,Rd}}$ (curve a)	$\frac{N_{FEM}}{N_{b,Rd}}$ (curve b)
Number of models #	300	300	300	300
Mean (P_m)	1.16	1.23	1.13	1.23
Standard deviation	0.05	0.05	0.064	0.066
COV (V_P)	0.045	0.047	0.057	0.054
Resistance factor (ϕ)	1.00	1.00	1.00	1.00
Correction factor (C_P)	1.01	1.01	1.01	1.01
Reliability index (β)	2.57	2.81	2.50	2.76

Table 5
Reliability analysis for the analytical prediction based on the EN1993-1-1, clause 6.4.3 [7] formulas.

Cold-formed battened columns	Fixed battened column		Pinned battened column	
	$\frac{N_{FEM}}{N_{b,Rd}}$ (curve a)	$\frac{N_{FEM}}{N_{b,Rd}}$ (curve b)	$\frac{N_{FEM}}{N_{b,Rd}}$ (curve a)	$\frac{N_{FEM}}{N_{b,Rd}}$ (curve b)
Number of models #	300	300	300	300
Mean (P_m)	1.10	1.13	1.08	1.15
Standard deviation	0.06	0.08	0.012	0.12
COV (V_P)	0.054	0.068	0.011	0.010
Resistance factor (ϕ)	1.00	1.00	1.00	1.00
Correction factor (C_P)	1.01	1.01	1.01	1.01
Reliability index (β)	2.33	2.41	2.10	2.30

models and analytical prediction following the EN1993-1-1, Clause 6.3.1 [7].

According to the EN1993-1-1, Clause 6.3.1 [7], the design resistance of the class-4 section under pure compression can be calculated by Eq. (3). Eq. (3) is directly related to the effective sectional area, calculated according to [5,64]. The design resistance of a class-4 member under pure compression can be calculated by multiplying a reduction factor by the design resistance of the section as Eq. (4). The reduction factor (χ) is calculated by Eq. (5), which is related to the design buckling curve (α) in Eq. (6) and the slenderness of the compression element (λ). The slenderness is obtained using Eq. (7), which depends on the effective section area and the minimum value among the elastic flexural, torsional, and torsional–flexural buckling forces. The elastic flexural buckling force is calculated using Eq. (8), where L_e is the total column length for the pined column and 50% of the column length for the fixed column.

A comparison was made between the obtained results from the finite element modeling and analytical formulas (EN1993-1-1, clause 6.3.1 [7]) for the fixed (Fig. 21**a**) and pinned (Fig. 21**b**) CFS built-up battened columns. Fig. 21 showed that the obtained results covered buckling *curve a* and above *curve b*, leading to a safe design by considering buckling *curve b*. However, it should be mentioned that the results for columns with intermediate slenderness (approximately $0.75 \leq \lambda \leq 1.5$), where the failure occurs due to the interaction between global and local is under the *curve a*, where is in agreement with previous studies in [18,19]. Moreover, it can be seen that the battened columns using the recommended batten panel distance ($30i_{min}$) and four rows of fasteners represent a full or close to full composite action and can be designed with the general methodology in the EN1993-1-1, clause 6.3.1 [7]. The ratio of the finite element model to the design buckling load (according to EN1993-1-1, clause 6.3.1 [7]) for various slenderness is shown in Fig. 22. As shown in Fig. 22**a**, the design buckling load considering buckling *curve a* is slightly unconservative, while a safe prediction is achieved by considering buckling *curve b*. Although a slightly unconservative prediction was seen for a few models, the overall mean value for the design prediction (1.08) shows an 8% difference on the safe side (Table 3). For the case of pinned battened columns (Fig. 22**b**), the design buckling load prediction considering buckling *curve a* is unsafe. At the same time, a safe prediction with an average of 13% is achieved by considering buckling *curve b*.

Table 3 lists detailed data for the reliability analysis for the analytical prediction according to EN1993-1-1, clause 6.3.1 [7]. As can be seen, the correction factor is 1.01, showing a suitable number of models to perform reliability analysis. The reliability index value for the analytical approach according to the EN1993-1-1, clause 6.3.1 [7] shows values less than 2.5 replicating an unreliable methodology. However, it is seen that the design prediction considering the buckling *curve b* represents a higher value of the reliability index, showing less unreliability than those considering the buckling *curve a*.

$$N_{c,Rd} = \frac{A_{eff} f_y}{\gamma_{M1}} \tag{3}$$

$$N_{b,Rd} = \chi N_{c,Rd} \tag{4}$$

$$\chi = 1/\left(\Phi + \sqrt{\Phi^2 - \bar{\lambda}^2}\right) \tag{5}$$

$$\Phi = 0.5\left[1 + \alpha\left(\bar{\lambda} - 0.2\right) + \bar{\lambda}^2\right] \tag{6}$$

$$\bar{\lambda} = \sqrt{\frac{A_{eff} f_y}{N_{cr}}}; \quad N_{cr} = \min\left\{N_{cr,F}, N_{cr,T}, N_{cr,FT}\right\} \tag{7}$$

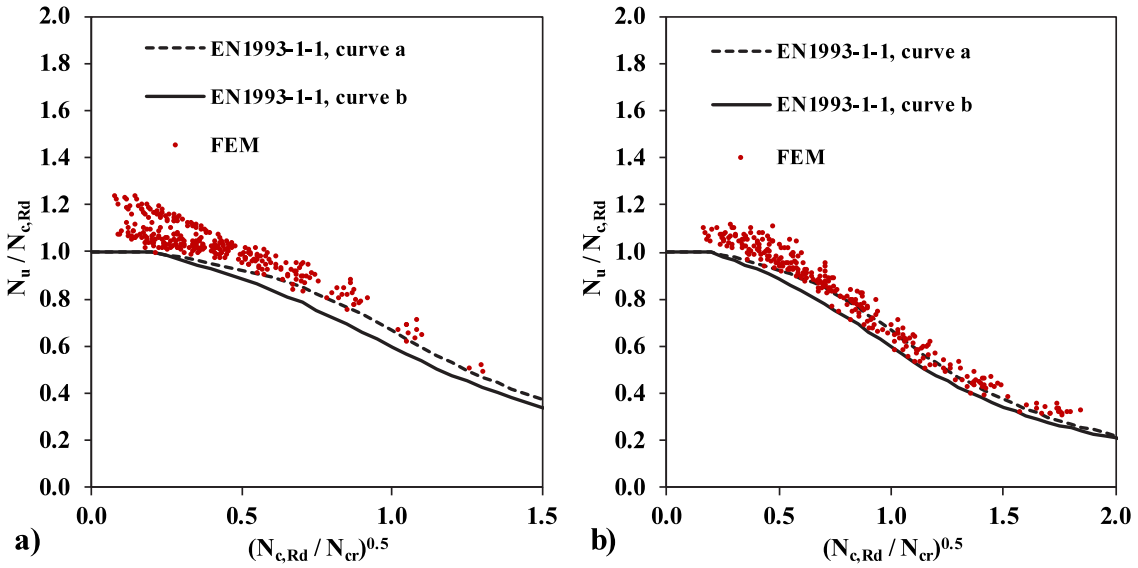

Fig. 21. Comparison between the obtained results from the finite element and analytical methods (EN1993-1-1, clause 6.3.1 [7]) for the battened columns with boundary conditions: **(a)** fixed and **(b)** pinned.

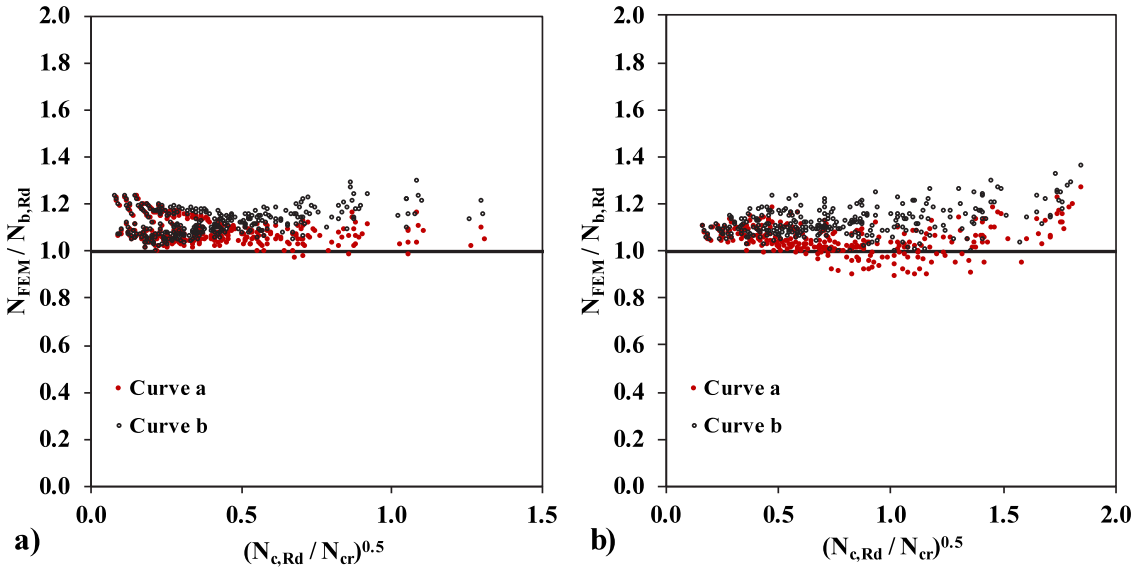

Fig. 22. Comparing axial buckling resistance obtained from the finite element models and the EN1993-1-1, clause 6.3.1 [7] for the battened columns with boundary conditions: **(a)** fixed and **(b)** pinned.

$$N_{cr,F} = \frac{\pi^2 EI}{L_e^2} = \frac{\pi^2 EA}{(L_e/r)^2} \tag{8}$$

4.4. The EN1993-1-1, clause 6.3.1 [7] incorporated the recommended slenderness ratio from the AISI S100-16 [6]

The North American Specification (NAS) AISI S100 [6] recommends increasing the slenderness ratio of the battened columns according to Eq. (9). In the recommended slenderness by the AISI S100 [6], the overall slenderness ratio is added by a ratio obtained from a distance between the batten panels and the minimum radius of gyration of the full unreduced cross-sectional area of an individual shape in a built-up member.

$$\left(\frac{KL}{r}\right)_m = \sqrt{\left(\frac{KL}{r}\right)_0^2 + \left(\frac{d_{bp}}{r_i}\right)^2} \tag{9}$$

Considering the recommended slenderness ratio, the EN1993-1-1, clause 6.3.1 [7] formulations (Eqs. (3)–(8)) can be replaced by Eqs. (10)–(14). The applicability of the EN1993-1-1, clause 6.3.1, by adopting the slenderness from the AISI S100 [6] was proposed in [8]. This combination successfully predicted the axial load-bearing capacity of a battened column made of C-shaped profiles.

$$N_{b,Rd}{}^{*} = \chi^{*} N_{c,Rd} \tag{10}$$

$$\chi^{*} = 1/\left(\Phi + \sqrt{\Phi^2 - \bar{\lambda}^2}\right) \tag{11}$$

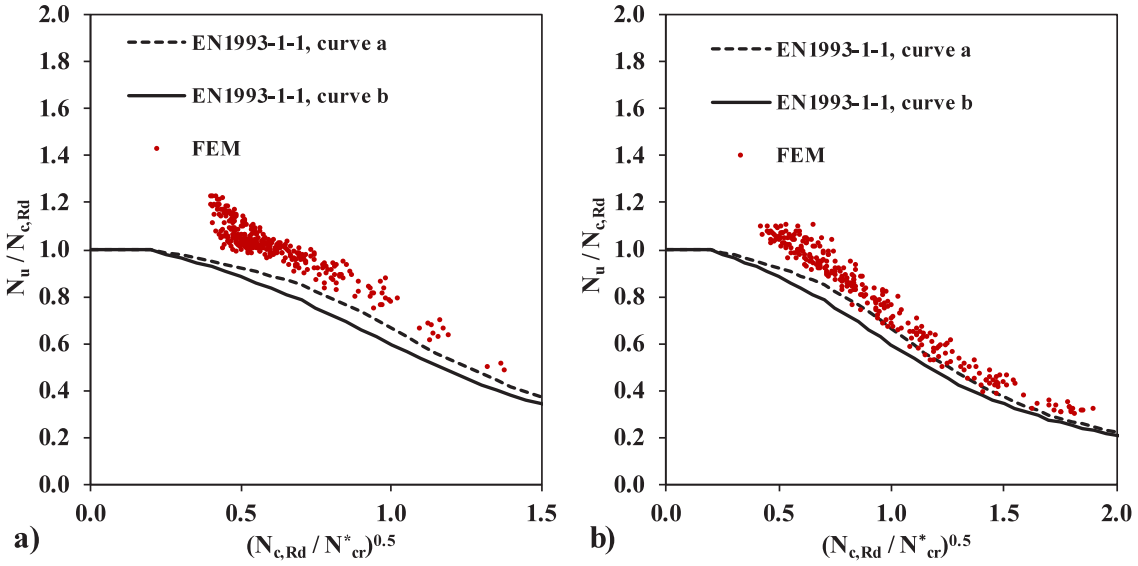

Fig. 23. Comparison between the obtained results from the finite element and analytical methods (the EN1993-1-1, clause 6.3.1 [7] incorporated with the recommended slenderness ratio from the AISI S100-16 [6]) for the battened columns with boundary conditions: **(a)** fixed and **(b)** pinned.

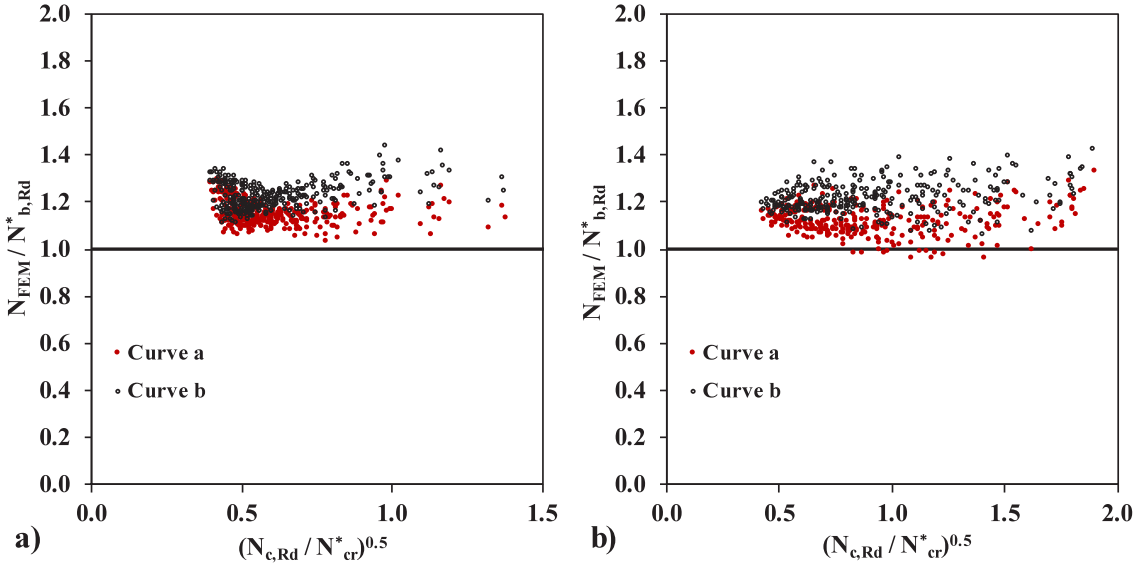

Fig. 24. Comparing axial buckling resistance obtained from the finite element models and the EN1993-1-1, clause 6.3.1 [7] incorporated with the recommended slenderness ratio from the AISI S100-16 [6] for the battened columns with boundary conditions: **(a)** fixed and **(b)** pinned.

$$\Phi^* = 0.5\left[1 + \alpha\left(\overline{\lambda}^* - 0.2\right) + \overline{\lambda}^{*2}\right] \tag{12}$$

$$\overline{\lambda}^* = \sqrt{\frac{A_{eff} f_y}{N_{cr}{}^*}}; \quad N_{cr} = \min\left\{N_{cr,F}{}^*, N_{cr,T}, N_{cr,FT}\right\} \tag{13}$$

$$N_{cr,F}{}^* = \frac{\pi^2 EA}{\left(\frac{L_e}{r}\right)_0^2 + \left(\frac{d_{bp}}{r_i}\right)^2} \tag{14}$$

A comparison was made between the finite element and analytical results (the EN1993-1-1, clause 6.3.1 [7] incorporated with the recommended slenderness ratio from the AISI S100-16 [6]) for the fixed (Fig. 23**a**) and pinned (Fig. 23**b**) CFS built-up battened columns. As shown in Fig. 23**a**, the fixed CFS built-up battened columns' results were above the buckling *curve a*. A similar result was seen for the pinned CFS built-up battened columns; however, the results for a few cases were slightly lower than the buckling *curve a*. The ratio obtained from the finite element models over those buckling loads calculated according to the EN1993-1-1, clause 6.3.1 [7] incorporated with the recommended slenderness ratio from the AISI S100-16 [6] is shown in Fig. 24. As shown in Fig. 24**a**, most of the design buckling load considering buckling *curve a* is well predicted the axial load-bearing capacity with a mean ratio of 1.16. At the same time, a conservative

prediction of up to 23% is obtained considering the buckling *curve b*. Similar results were obtained for the pinned CFS built-up battened columns (Fig. 24**b**).

According to Section 4.2, the reliability analysis was performed and presented in Table 4 to evaluate the reliability of the methodology presented in the EN1993-1-1, clause 6.3.1 [7] incorporated with the recommended slenderness ratio from the AISI S100-16 [6] for the CFS built-up battened columns. It is seen that the reliability index is higher than 2.5 for all situations. However, it is worth mentioning that the reliability index for the methodology based on the EN1993-1-1, clause 6.3.1 [7] incorporated with the recommended slenderness ratio from the AISI S100-16 [6] and considering buckling *curve b* is higher than those considering buckling *curve a*, resulting in more reliable prediction by considering buckling *curve b*.

4.5. Methodology in the EN1993-1-1, clause 6.4.3 [7]

The EN1993-1-1 [7] presents a design methodology for calculating the design buckling resistance of the CFS built-up battened columns following clause 6.4.3. Note that the method available in EN1993-1-1, clause 6.4.3 [7], is according to the recommendations provided by the ECCS [65]. In general, this methodology, in particular, determines the slenderness of the battened column, as presented in Eq. (15). The critical load ($N_{cr,B}$) is calculated according to Eq. (16), where the Elastic flexural buckling force of the effective battened column is obtained from Eq. (17) and assessed considering a reduced moment of inertia (I_{eff}). The reduced moment of inertia can be determined according to Eqs. (18)–(20). Moreover, the shear stiffness of the built-up member from the batten panel is determined using Eq. (21).

Fig. 25 compares the obtained results from the finite element and analytical methods (EN1993-1-1, clause 6.4.3 [7]). For both fixed and pinned boundary conditions, the results followed the buckling *curve a* or between buckling *curves a* and *b*. However, the EN1993-1-1, clause 6.4.3 [7] recommended buckling *curve b* for calculating the reduction factor. A comparison was made between the maximum axial load-bearing capacity from the finite element model and design buckling load prediction by EN1993-1-1, clause 6.4.3 [7], as shown in Fig. 26. It is seen that the design buckling load predicted using the EN1993-1-1, clause 6.4.3 [7], considering buckling *curve b* is safe.

Table 5 lists detailed data for the reliability analysis for the analytical prediction according to EN1993-1-1, clause 6.3.1 [7]. The reliability index value for the analytical approach, according to the EN1993-1-1, clause 6.3.1 [7], shows values less than 2.5. These low values for the reliability index replicate the unreliable prediction provided by EN1993-1-1, clause 6.3.1 [7].

$$\overline{\lambda^{**}} = \sqrt{\frac{A_{eff} f_y}{N_{cr,B}}} \tag{15}$$

$$N_{cr,B} = \frac{1}{\frac{1}{N_{cr,eff}} + \frac{1}{S_v}} \tag{16}$$

$$N_{cr,eff} = \frac{\pi^2 E I_{eff}}{L_e^2} \tag{17}$$

$$I_{eff} = 0.5 h_0^2 A_{ch} + 2\mu I_{ch} \tag{18}$$

$$\mu = \begin{cases} 0, & \lambda \geq 150 \\ 2 - \frac{\lambda}{75}, & 75 < \lambda < 150 \\ 1.0, & \lambda \leq 75 \end{cases} \tag{19}$$

$$\lambda = \frac{L}{i_0};\ i_0 = \sqrt{\frac{I_1}{2\,A_{ch}}};\ I_1 = 0.5 h_0^2 A_{ch} + 2 I_{ch} \tag{20}$$

$$S_v = \frac{24 E I_{ch}}{{d_{bp}}^2 \left[1 + \frac{2 I_{ch}}{n_b I_{bp}} \frac{h_0}{d_{bp}}\right]} \leq \frac{2\pi^2 E I_{ch}}{{b_{bp}}^2} \tag{21}$$

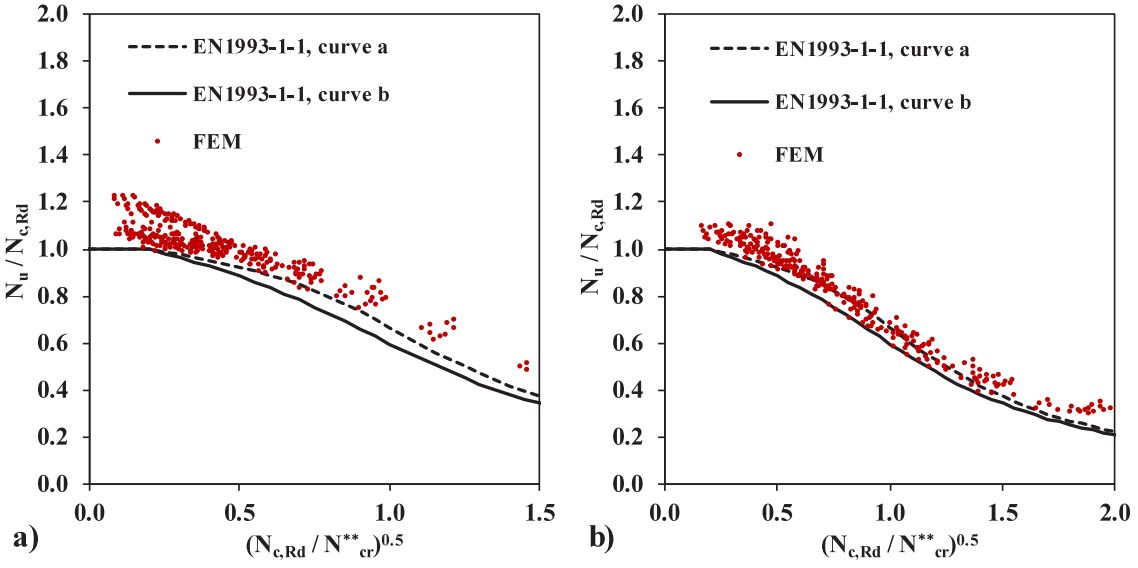

Fig. 25. Comparison between the obtained results from the finite element and analytical methods (EN1993-1-1, clause 6.4.3 [7]) for the battened columns with boundary conditions: **(a)** fixed, **(b)** pinned.

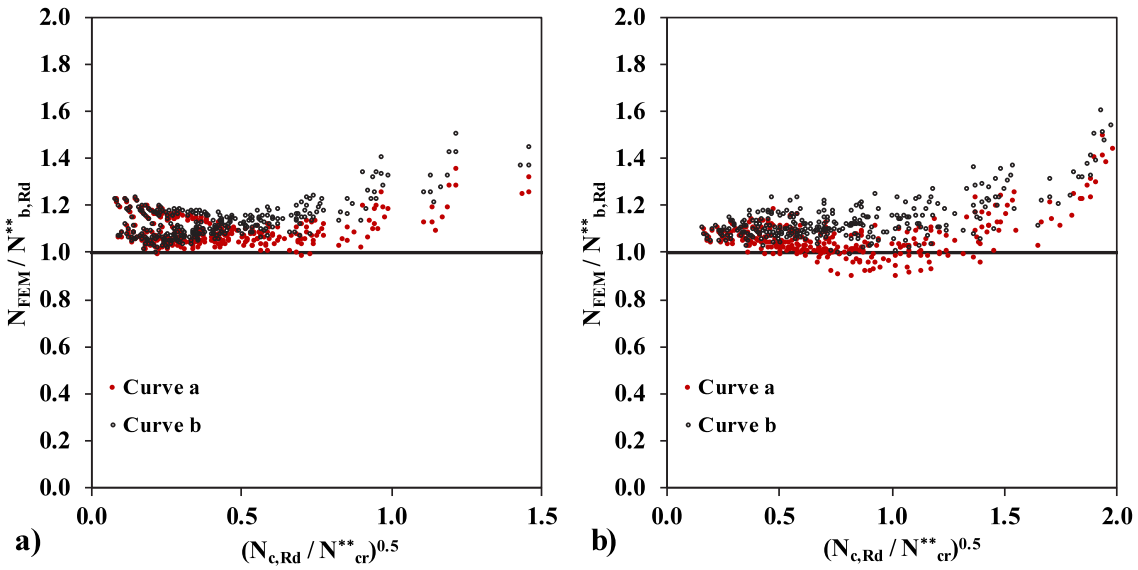

Fig. 26. Comparing axial buckling resistance obtained from the finite element models and the EN1993-1-1, clause 6.4.3 [7] for the battened columns with boundary conditions: **(a)** fixed and **(b)** pinned.

5. Conclusions

The compression behavior of various CFS built-up battened columns (700 models) was investigated in this study. The modeling techniques were verified by comparing axial force vs. shortening displacement obtained from numerical models and experimental specimens [10,30,61]. The initial imperfection was defined using global and local buckling modes. The optimal number of fastener rows per batten panel and the optimal distance between batten panels along the CFS built-up battened columns were investigated through 100 finite element models. These suggestions were determined to achieve full or close to full composite action between two individual CFS profiles. Five different *h/b* ratios were considered in all steps of the investigation. After defining the optimal layout for the CFS built-up battened columns, a parametric study was conducted using 600 finite element models to investigate the accuracy of the available methodologies in the European Standards.

The findings are summarized as follows:

1. The results recommended $30i_{min}$ as the distance between batten panels along the column, fastened using four rows of fasteners per batten panel. The results showed these values as optimal to achieve the full or close to full composite action between two Σ-shaped cold-formed steel profiles. This recommended distance between batten panels along the column agrees with the previous finding [8,9].
2. Comparing finite element results and analytical procedures based on the EN1993-1-1, clause 6.3.1 [7] showed unconservative results for the CFS built-up section with batten panels when buckling *curve a* is considered. At the same time, the analytical prediction considering buckling *curve b* was safe. Note that the analytical prediction taking the buckling *curve-a* into account represents a correct procedure, and only slightly unconservative results were found for a few cases.
3. The applicability of the EN1993-1-1, clause 6.3.1 [7], by adopting the slenderness from the AISI S100 [6] was proposed in [8]. Its applicability for the presented battened columns fabricated using Σ-shaped cold-formed steel profiles was investigated, resulting in good accuracy. This study recommends the slenderness from the AISI S100 [6] used in the EN1993-1-1, clause 6.3.1 [7], to predict the axial capacity of battened built-up columns. This paper showed that slenderness from the AISI S100 [6] used in the EN1993-1-1, clause 6.3.1 [7] could accurately predict the axial capacity of the CFS built-up battened columns when buckling *curve a* is considered. However, the reliability analysis achieved a higher reliability index (β = 2.81 for fixed and β = 2.76 for pinned) when buckling *curve b* was used to predict the axial capacity.
4. The EN1993-1-1 [7] proposed a methodology for battened columns in clause 6.4.3. Buckling *curve b* also was suggested in the EN1993-1-1, clause 6.4.3 [7]. Its applicability for battened columns fabricated using Σ-shaped cold-formed steel profiles was investigated. The results showed that the predictions provided by formulation in the EN1993-1-1, clause 6.4.3 [7], were conservative in general. However, the reliability index for its prediction (<2.5) represented clause 6.4.3 as an unreliable procedure.

6. Future work

Although research studies were conducted on CFS built-up battened columns, many details are still missing to present a fully reliable design methodology. The compression behavior of CFS built-up battened columns can be explored more when the batten panels are positioned in the minor axis of the columns. Therefore, more experimental, numerical, and analytical are suggested for future studies to address more remained details of the CFS built-up battened columns. It was concluded in Section 3.1 that increasing the axial load-bearing capacity due to the number of fasteners also included the effect of the batten panel's stiffness. The contribution of the fasteners and the plate stiffness can be addressed in more detail in future studies. Although four fastener rows per batten panel are suggested in this study, an investigation of the design procedure of batten panels is recommended in which the required fasteners for the batten panel connection are determined by computing the required resistance of connections between the profiles, the batten panels, and the shear resistance of each fastener.

CRediT authorship contribution statement

Rohola Rahnavard: Visualization, Validation, Software, Methodology, Investigation, Formal analysis, Data curation, Conceptualization, Writing – original draft, Writing – review & editing. **Mahtabsadat Razavi:** Writing – review & editing, Software, Formal analysis. **Nader Fanaie:** Writing – review & editing. **Hélder D. Craveiro:** Supervision, Writing – review & editing.

Declaration of competing interest

The authors declare that they have no known competing financial interests or personal relationships that could have appeared to influence the work reported in this paper.

Data availability

The authors do not have permission to share data.

Acknowledgments

This work is financed by national funds through Portuguese Foundation for Science and Technology (FCT), under grant agreement 2021.06528.BD attributed to the 1st author and under the grant agreement
2020.03588.CEECIND attributed to the 4th author.

The authors gratefully acknowledge the Portuguese Foundation for Science and Technology (FCT) for its support under the framework of the research project PTDC/ECI- EGC/31858/2017 – INNOCFSCONC – Innovative hybrid structural solutions using cold- formed steel and lightweight concrete", financed by FEDER funds through the Competitivity Factors Operational Programme-COMPETE and by national funds through FCT and D_INNOCFSCONC – "Demonstração de Solução Estrutural Híbrida Inovadora com Recurso a Aço-Enformado a Frio e Betão Leve", funded by the call for starting projects and proof of concept projects UI-Transfer, with operation Code POCI-01-0246-FEDER-181315 financed by COMPETE 2020.

This work was partly financed by FCT/MCTES through national funds (PIDDAC) under the R&D Unit Institute for Sustainability and Innovation in Structural Engineering (ISISE), under reference UIDB/04029/2020.

References

[1] Ioannis Papargyriou, Iman Hajirasouliha, Jurgen Becque, Kypros Pilakoutas, Performance-based assessment of CFS strap-braced stud walls under seismic loading, J. Construct. Steel Res. 183 (2021) 106731, http://dx.doi.org/10.1016/j.jcsr.2021.106731.

[2] Ornella Iuorio, Vincenzo Macillo, Maria Teresa Terracciano, Tatiana Pali, Luigi Fiorino, Raffaele Landolfo, Seismic response of Cfs strap-braced stud walls: Experimental investigation, Thin-Walled Struct. 85 (2014) 466–480, http://dx.doi.org/10.1016/j.tws.2014.09.008.

[3] Shuna Ni, Xia Yan, Matthew S. Hoehler, Thomas Gernay, Numerical modeling of the post-fire performance of strap-braced cold-formed steel shear walls, Thin-Walled Struct. 171 (2022) 108733, http://dx.doi.org/10.1016/j.tws.2021.108733.

[4] Luís Simões da Silva, Luís Carlos Silva, Trayana Tankova, Hélder David Craveiro, Rui Simões, Ricardo Costa, Mario D'Aniello, Raffaele Landolfo, Performance of modular hybrid cold-formed/tubular structural system, Structures 30 (2021) 1006–1019, http://dx.doi.org/10.1016/j.istruc.2021.01.066.

[5] CEN, Eurocode 3, Design of Steel Structures-Part 1-3: General Rules- Supplementary Rules for Cold-Formed Members and Sheeting, European Committee for Standardization, Brussels, 2006.

[6] AISI, North American Specification for the Design of Cold-Formed Steel Structural Members, 2016.

[7] CEN, Eurocode 3, Design of Steel Structures- Part 1-1: General Rules and Rules for Building, European Committee for Standardization, Brussels, 2005.

[8] Rohola Rahnavard, Hélder D. Craveiro, Rui A. Simões, Design of Cold-Formed Steel Battened Built-Up Columns, Cold-Formed Steel Research Consortium (CFSRC) Colloquium, 2022.

[9] Rohola Rahnavard, Hélder D. Craveiro, Luís Laím, Rui A. Simões, Rebecca Napolitano, Numerical investigation on the composite action of cold-formed steel built-up battened columns, Thin-Walled Struct. 162 (2021) 107553, http://dx.doi.org/10.1016/j.tws.2021.107553.

[10] M. Adil Dar, Dipti Ranjan Sahoo, Arvind K. Jain, Abhishek Verma, Tests on CFS laced columns composed of plain channels: Behavior and design, J. Struct. Eng. 148 (5) (2022) http://dx.doi.org/10.1061/(ASCE)ST.1943-541X.0003329.

[11] A.R. Dar, S. Vijayanand, M. Anbarasu, M.A. Dar, Cold-formed steel battened built-up columns: Experimental behaviour and verification of different design rules developed, Adv. Struct. Eng. 25 (2) (2022) 321–335, http://dx.doi.org/10.1177/13694332211048006.

[12] M. Adil Dar, Dipti Ranjan Sahoo, Sunil Pulikkal, Arvind K. Jain, Behaviour of laced built-up cold-formed steel columns: Experimental investigation and numerical validation, Thin-Walled Struct. 132 (2018) 398–409, http://dx.doi.org/10.1016/j.tws.2018.09.012.

[13] M. Adil Dar, Abhishek Verma, M. Anbarasu, Sze Dai Pang, A.R. Dar, Design of cold-formed steel battened built-up columns, J. Construct. Steel Res. 193 (2022) 107291, http://dx.doi.org/10.1016/j.jcsr.2022.107291.

[14] A.R. Dar, S. Vijayanand, M. Anbarasu, M.A. Dar, Cold-formed steel battened built-up columns: Experimental behaviour and verification of different design rules developed, Adv. Struct. Eng. 25 (2) (2022) 321–335, http://dx.doi.org/10.1177/13694332211048006.

[15] M. Adil Dar, Dipti Ranjan Sahoo, Arvind K. Jain, Saurabh Sharma, Monotonic tests and numerical validation of cold-formed steel battened built-up columns, Thin-Walled Struct. 159 (2021) 107275, http://dx.doi.org/10.1016/j.tws.2020.107275.

[16] M. Adil Dar, N. Subramanian, M. Anbarasu, Ahmad Fayeq Ghowsi, P. Azmat Arif, A.R. Dar, Testing and FE simulation of lightweight CFS composite built-up columns: Axial strength and deformation behaviour, Thin-Walled Struct. 167 (2021) 108222, http://dx.doi.org/10.1016/j.tws.2021.108222.

[17] Wilson Reyes, Andrés Guzmán, Evaluation of the slenderness ratio in built-up cold-formed box sections, J. Construct. Steel Res. 67 (6) (2011) 929–935, http://dx.doi.org/10.1016/j.jcsr.2011.02.003.

[18] Mohamed Dabaon, Ehab Ellobody, Khaled Ramzy, Nonlinear behaviour of built-up cold-formed steel section battened columns, J. Construct. Steel Res. 110 (2015) 16–28, http://dx.doi.org/10.1016/j.jcsr.2015.03.007.

[19] Mohamed Dabaon, Ehab Ellobody, Khaled Ramzy, Experimental investigation of built-up cold-formed steel section battened columns, Thin-Walled Struct. 92 (2015) 137–145, http://dx.doi.org/10.1016/j.tws.2015.03.001.

[20] Khaled Ramzy, Mohamed Dabaon, Mahmoud El-Boghdadi, Experimental tests on built-up cold-formed steel section laced compression members, Thin-Walled Struct. 172 (2022) 108882, http://dx.doi.org/10.1016/j.tws.2021.108882.

[21] AS/NZS. Australian/New Zealand Standard, Cold-Formed Steel Structures, Standards Australia, Sydney, Australia, 1996.

[22] M.A. El Aghoury, A.H. Salem, M.T. Hanna, E.A. Amoush, Experimental investigation for the behaviour of battened beam–columns composed of four equal slender angles, Thin-Walled Struct. 48 (9) (2010) 669–683, http://dx.doi.org/10.1016/j.tws.2010.03.007.

[23] M.A. El Aghoury, A.H. Salem, M.T. Hanna, E.A. Amoush, Ultimate capacity of battened columns composed of four equal slender angles, Thin-Walled Struct. 63 (2013) 175–185, http://dx.doi.org/10.1016/j.tws.2012.07.019.

[24] M.A. El Aghoury, A.H. Salem, M.T. Hanna, E.A. Amoush, Strength of cold formed battened columns subjected to eccentric axial compressive force, J. Construct. Steel Res. 113 (2015) 58–70, http://dx.doi.org/10.1016/j.jcsr.2015.04.008.

[25] M. Anbarasu, M. Adil Dar, Improved design procedure for battened cold-formed steel built-up columns composed of lipped angles, J. Construct. Steel Res. 164 (2020) 105781, http://dx.doi.org/10.1016/j.jcsr.2019.105781.

[26] David C. Fratamico, Shahabeddin Torabian, Xi Zhao, Kim J.R. Rasmussen, Benjamin W. Schafer, Experiments on the global buckling and collapse of built-up cold-formed steel columns, J. Construct. Steel Res. 144 (2018) 65–80, http://dx.doi.org/10.1016/j.jcsr.2018.01.007.

[27] David C. Fratamico, Shahabeddin Torabian, Xi Zhao, Kim J.R. Rasmussen, Benjamin W. Schafer, Experimental study on the composite action in sheathed and bare built-up cold-formed steel columns, Thin-Walled Struct. 127 (2018) 290–305, http://dx.doi.org/10.1016/j.tws.2018.02.002.

[28] Jia-Hui Zhang, Ben Young, Compression tests of cold-formed steel I-shaped open sections with edge and web stiffeners, Thin-Walled Struct. 52 (2012) 1–11, http://dx.doi.org/10.1016/j.tws.2011.11.006.

[29] Jia-Hui Zhang, Ben Young, Numerical investigation and design of cold-formed steel built-up open section columns with longitudinal stiffeners, Thin-Walled Struct. 89 (2015) 178–191, http://dx.doi.org/10.1016/j.tws.2014.12.011.

[30] Jia-Hui Zhang, Ben Young, Experimental investigation of cold-formed steel built-up closed section columns with web stiffeners, J. Construct. Steel Res. 147 (2018) 380–392, http://dx.doi.org/10.1016/j.jcsr.2018.04.008.

[31] Ben Young, Research on cold-formed steel columns, Thin-Walled Struct. 46 (7–9) (2008) 731–740, http://dx.doi.org/10.1016/j.tws.2008.01.025.

[32] Mithum Peiris, Mahen Mahendran, Behaviour of cold-formed steel lipped channel sections subject to eccentric axial compression, J. Construct. Steel Res. 184 (2021) 106808, http://dx.doi.org/10.1016/j.jcsr.2021.106808.

[33] Tekcham Gishan Singh, Konjengbam Darunkumar Singh, Design of perforated cold-formed steel hollow stub columns using direct strength method, Thin-Walled Struct. 168 (2021) 108265, http://dx.doi.org/10.1016/j.tws.2021.108265.

[34] Naoual Djafour, Soumia Kherbouche, Abdellatif Megnounif, Parametric study on cold-formed steel built-up columns using direct strength method, Structures 39 (2022) 337–350, http://dx.doi.org/10.1016/j.istruc.2022.03.028.

[35] Qiu-Yun Li, Ben Young, Design of cold-formed steel built-up open section members under combined compression and bending, Thin-Walled Struct. 172 (2022) 108890, http://dx.doi.org/10.1016/j.tws.2022.108890.
[36] Ziqi He, Haoyuan Cao, Xuhong Zhou, Qixiu Li, Benjamin W. Schafer, Performance of cold-formed C-sections reinforced by sleeves under concentric and eccentric compression, J. Construct. Steel Res. 198 (2022) 107554, http://dx.doi.org/10.1016/j.jcsr.2022.107554.
[37] Kim J.R. Rasmussen, Mani Khezri, Benjamin W. Schafer, Hao Zhang, The mechanics of built-up cold-formed steel members, Thin-Walled Struct. 154 (2020) 106756, http://dx.doi.org/10.1016/j.tws.2020.106756.
[38] M. Abbasi, M. Khezri, K.J.R. Rasmussen, B.W. Schafer, Elastic buckling analysis of cold-formed steel built-up sections with discrete fasteners using the compound strip method, Thin-Walled Struct. 124 (2018) 58–71, http://dx.doi.org/10.1016/j.tws.2017.11.046.
[39] Iveta Georgieva, Luc Schueremans, Lincy Pyl, Composed columns from cold-formed steel Z-profiles: Experiments and code-based predictions of the overall compression capacity, Eng. Struct. 37 (2012) 125–134, http://dx.doi.org/10.1016/j.engstruct.2011.12.017.
[40] Iveta Georgieva, Luc Schueremans, Lincy Pyl, Lucie Vandewalle, Experimental investigation of built-up double-z members in bending and compression, Thin-Walled Struct. 53 (2012) 48–57, http://dx.doi.org/10.1016/j.tws.2011.12.017.
[41] Iveta Georgieva, Luc Schueremans, Lincy Pyl, Lucie Vandewalle, Numerical study of built-up double-z members in bending and compression, Thin-Walled Struct. 60 (2012) 85–97, http://dx.doi.org/10.1016/j.tws.2012.07.005.
[42] I. Georgieva, L. Schueremans, L. Vandewalle, L. Pyl, Design of built-up cold-formed steel columns according to the direct strength method, Procedia Eng. 40 (2012) 119–124, http://dx.doi.org/10.1016/j.proeng.2012.07.066.
[43] Paweł Lorkowski, Bronisław Gosowski, Experimental and numerical research of the torsion problem of built-up steel columns laced in a single plane, Eng. Struct. 160 (2018) 566–580, http://dx.doi.org/10.1016/j.engstruct.2018.01.049.
[44] Krishanu Roy, Chia Mohammadjani, James B.P. Lim, Experimental and numerical investigation into the behaviour of face-to-face built-up cold-formed steel channel sections under compression, Thin-Walled Struct. 134 (2019) 291–309, http://dx.doi.org/10.1016/j.tws.2018.09.045.
[45] T.C.H. Ting, K. Roy, H.H. Lau, J.B. Lim, Effect of screw spacing on behavior of axially loaded back-to-back cold-formed steel built-up channel sections, Adv. Struct. Eng. 21 (3) (2018) 474–487, http://dx.doi.org/10.1177/1369433217719986.
[46] M. Muthuraman, R. Anuradha, P.O. Awoyera, R. Gobinath, Numerical simulation and specification provisions for buckling characteristics of a built-up steel column section subjected to axial loading, Eng. Struct. 207 (2020) 110256, http://dx.doi.org/10.1016/j.engstruct.2020.110256.
[47] Jessica Whittle, Chris Ramseyer, Buckling capacities of axially loaded, cold-formed, built-up C-channels, Thin-Walled Struct. 47 (2) (2009) 190–201, http://dx.doi.org/10.1016/j.tws.2008.05.014.
[48] Yuanqi Li, Yinglei Li, Shukun Wang, Zuyan Shen, Ultimate load-carrying capacity of cold-formed thin-walled columns with built-up box and I section under axial compression, Thin-Walled Struct. 79 (2014) 202–217, http://dx.doi.org/10.1016/j.tws.2014.02.003, m.
[49] Hélder D. Craveiro, João Paulo C. Rodrigues, Luís Laím, Buckling resistance of axially loaded cold-formed steel columns, Thin-Walled Struct. 106 (2016) 358–375, http://dx.doi.org/10.1016/j.tws.2016.05.010.
[50] Xuhong Zhou, Ming Chen, Experimental investigation and finite element analysis of web-stiffened cold-formed lipped channel columns with batten sheets, Thin-Walled Struct. 125 (2018) 38–50, http://dx.doi.org/10.1016/j.tws.2018.01.006.
[51] Francisco J. Meza, Jurgen Becque, Iman Hajirasouliha, Experimental study of cold-formed steel built-up columns, Thin-Walled Struct. 149 (2020) 106291, http://dx.doi.org/10.1016/j.tws.2019.106291.
[52] Francisco J. Meza, Jurgen Becque, Iman Hajirasouliha, Experimental study of the cross-sectional capacity of cold-formed steel built-up columns, Thin-Walled Struct. 155 (2020) 106958, http://dx.doi.org/10.1016/j.tws.2020.106958.
[53] Jun Ye, Iman Hajirasouliha, Jurgen Becque, Experimental investigation of local-flexural interactive buckling of cold-formed steel channel columns, Thin-Walled Struct. 125 (2018) 245–258, http://dx.doi.org/10.1016/j.tws.2018.01.020.
[54] Seyed Mohammad Mojtabaei, Jurgen Becque, Iman Hajirasouliha, Structural size optimization of single and built-up cold-formed steel beam-column members, J. Struct. Eng. 147 (2021) 04021030, http://dx.doi.org/10.1061/(ASCE)ST.1943-541X.0002987.
[55] S.J. Qadir, V.B. Nguyen, I. Hajirasouliha, B. Cartwright, M.A. English, Optimal design of cold roll formed steel channel sections under bending considering both geometry and cold work effects, Thin-Walled Struct. 157 (2020) 107020, http://dx.doi.org/10.1016/j.tws.2020.107020.
[56] Jurgen Becque, Kim J.R. Rasmussen, Experimental investigation of local-overall interaction buckling of stainless steel lipped channel columns, J. Construct. Steel Res. 65 (8–9) (2009) 1677–1684, http://dx.doi.org/10.1016/j.jcsr.2009.04.025.
[57] Abaqus User's Manual, 2011.
[58] Rohola Rahnavard, Hélder D. Craveiro, Rui A. Simões, Luís Laím, Aldina Santiago, Buckling resistance of concrete-filled cold-formed steel (CF-CFS) built-up short columns under compression, Thin-Walled Struct. 170 (2022) 108638, http://dx.doi.org/10.1016/j.tws.2021.108638.
[59] Hélder D. Craveiro, João Paulo C. Rodrigues, Aldina Santiago, Luís Laím, Review of the high temperature mechanical and thermal properties of the steels used in cold formed steel structures – The case of the S280 Gd+Z steel, Thin-Walled Struct. 98 (Part A) (2016) 154–168, http://dx.doi.org/10.1016/j.tws.2015.06.002.
[60] Hélder David da Silva Craveiro, Fire Resistance of Cold-Formed Steel Columns (PHD thesis), ISISE-Depatment of Civil Engineering, University of Coimbra, Portugal, 2016.
[61] Hélder D. Craveiro, Rohola Rahnavard, Luís Laím, Rui A. Simões, Aldina Santiago, Buckling behavior of closed built-up cold-formed steel columns under compression, Thin-Walled Struct. 179 (2022) 109493, http://dx.doi.org/10.1016/j.tws.2022.109493.
[62] Minh Toan Huynh, Cao Hung Pham, Gregory J. Hancock, Experimental behaviour and modelling of screwed connections of high strength sheet steels in shear, Thin-Walled Struct. 146 (2020) 106357, http://dx.doi.org/10.1016/j.tws.2019.106357.
[63] Guan Quan, Jun Ye, Wenchao Li, Computational modelling of Cold-formed steel lap joints with screw fasteners, Structures 33 (2021) 230–245, http://dx.doi.org/10.1016/j.istruc.2021.04.062.
[64] CEN, Eurocode 3, Design of Steel Structures-Part 1-5: Plated Structural Elements, European Committee for Standardisation, Brussels, Belgium, 2006.
[65] CECM ECCS, European Recommendations for Steel Construction, ECCS, Brussels, 1978.